Charles University in Prague
Faculty of Mathematics and Physics

DIPLOMA THESIS

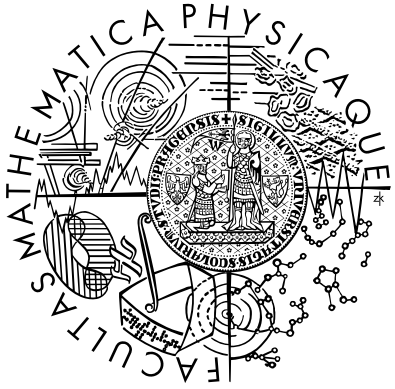

Jan Alster

Excited states relaxation in artificial photosynthetic antenna

Department of Chemical Physics and Optics
Supervisor: **Doc. RNDr. Jakub Pšenčík, Ph.D.**
Programme of study: **Physics**
Branch of study: **Biophysics and chemical physics**

First of all I would like to thank very much to my supervisor, Doc. RNDr. Jakub Pšenčík, Ph.D., for his indispensable guidance and advice concerning many aspects of my work.

I would like to thank to the people from the Department of Photosynthesis, Biological centre ASCR, Institute of Plant Molecular Biology, especially its head Doc. RNDr. František Vácha, PhD., for granting access to their apparatus. My thanks belong in particular to Mgr. David Bína and Mgr. Radek Litvín for their assistance in difference absorption spectroscopy experiments and to Mgr. Anita Župčanová for her help with pigment extraction.

I would also like to thank to members of Division of Biomolecular Physics of the Institute of Physics of Charles University for giving me the admission to their chemical laboratory.

Most of all I would like to express me gratitude to my family for their unwavering support throughout my studies.

I hereby declare, that I have written this diploma thesis independently using no other than cited references. I give my consent to this work being available on loan.

Prague April 21, 2006 Jan Alster

Contents

Název práce: *Relaxace excitonových stavů v umělé fotosyntetické anténě*
Autor: *Jan Alster*
Katedra (ústav): *Katedra chemické fyziky a optiky*
Vedoucí diplomové práce: *Doc. RNDr. Jakub Pšenčík, Ph.D.*
E-mail vedoucího: *psencik@karlov.mff.cuni.cz*
Abstrakt: *Relaxace excitonových stavů ve světlosběrné anténě zelené fotosyntetické bakterie Chlorobium tepidum, tzv. chlorosomu, a v umělé, chlorosomu podobné anténě, byla zkoumána za oxidujících a redukujících podmínek. K přípravě umělých antén založených na agregátech bakteriochlorofylu c (BChl c) byly využity doposud nepoužívané chemické složky. Je známo, že za oxidujících podmínek je excitace v chlorosomech zhášena procesem, pro který jsou důležité chinony a jehož mechanismus není objasněn. Na základě známých výsledků jsme navrhli tento mechanismus zhášení: za vyšších redoxních potenciálů způsobených přítomností kyslíku dojde k přenosu elektronu z excitovaného BChl c na molekulu chinonu a vzniklý BChl-ový kationt poté zháší excitační energii. Tato hypotéza byla testována pomocí fluorescenční a transientní absorpční spektroskopie. Pomocí fluorescenční spektroskopie byla potvrzena existence zhášení za vyšších redoxních potenciálů a jeho závislost na přítomnosti chinonů i v uměle připravených anténách. V transientních absorpčních spektrech byl za vyšších redoxních potenciálů pozorován vznik kationtů BChl c^+ a Car^+ na úkor neutrálních forem obou pigmentů. Jejich výskyt byl intenzivnější po přidání umělých akceptorů elektronů. Za nízkých redoxních potenciálů naopak přítomnost kationtů pozorována nebyla. Kinetika procesu byla tvořena dvěma složkami. Získané výsledky jsou ve shodě s navrženým mechanismem zhášení.*
Klíčová slova: *Chlorobium tepidum, světlosběrná anténa, zhášení excitační energie, chinon, kationt pigmentu*

Title: *Excited states relaxation in artificial photosynthetic antenna*
Author: *Jan Alster*
Department: *Department of Chemical Physics and Optics*
Supervisor: *Doc. RNDr. Jakub Pšenčík, Ph.D.*
Supervisor's e-mail address: *psencik@karlov.mff.cuni.cz*
Abstract: *Excitation energy relaxation in light harvesting antennae of green photosynthetic bacterium Chlorobium tepidum, so-called chlorosomes, and in artificial chlorosome-like antennae was studied under oxidizing and reducing conditions. The artificial antennae based on aggregates of bacteriochlorophyll c (BChl c) were prepared using novel components. It is known that under oxidizing conditions the excitation energy in chlorosomes is quenched in a process, for which a presence of quinones is important, however, the mechanism is not known yet. We propose that at higher redox potentials the excitation of BChl aggregate may be followed by electron transfer from BChl to a quinone molecule. The formed BChl c^+ acts as a quencher of the excitation energy. This hypothesis was tested using fluorescence and transient absorption spectroscopy. Using fluorescence spectroscopy, it was confirmed that the redox-dependent quenching might be induced by addition of quinones also in the artificial antennae. Formation of BChl c^+ and Car^+ at the expanse of neutral forms of both pigments was observed in transient absorption spectra. The formation of cations was enhanced by addition of artificial electron acceptors, while at low redox potentials cations were not observed. The formation of cations was characterized by two kinetic components. The obtained data are in accordance with the proposed mechanism of the quenching.*
Keywords: *Chlorobium tepidum, light-harvesting antenna, excitation energy quenching, quinone, pigment cation*

1 Introduction

Photosynthesis is the main source of energy for life on Earth. Understanding of photosynthetic processes and their adaptation in artificially created light-to-energy converters would provide a truly renewable and long-lasting source of energy for civilization.

The first steps of light conversion into chemical energy are capture of light quantum in light harvesting antennae and transfer of this excitation energy towards reaction centre.

1.1 Green sulphur bacteria

Green sulphur bacteria are photosynthetic anaerobic organisms typically living in seas, eutrophic lakes or in soil deep enough to ensure sufficiently low concentration of oxygen. Incident light intensity in such habitats is not very high, therefore the bacteria must exhibit high probability of photons capture. For that reason they have developed an unique light harvesting antennae, called chlorosomes.

Chlorosomes are ovoid objects ($150 \times 50 \times 20\,\mathrm{nm}$) attached to cell membrane containing reaction centres (RC). They consist of pigments, lipids (monogalactosyl diglyceride (MGDG)), quinones (1'-oxomenaqionone-7 (chlorobiumquinone), menaquinone-7), and proteins. The main pigments are bacteriochlorophyll *c*, *d*, *e* (BChl), depending on the strain of bacteria, carotenoids (Car) (chlorobactene), and a small amount of BChl *a*. It is believed that lipids form a mono-layer separating non polar interior of the chlorosome from polar environment inside cell, and that all proteins are inside this layer. Pigments in the chlorosome are held in position optimal for capturing photons not by protein matrix, but by pigment-pigment interactions; that is the unique property of chlorosomes.

Inessentiality of proteins for a chlorosome interior structure is enabled by the ability of BChl *c* to self-assembly (we use BChl *c* as a representative, BChl *d*, *e* have similar properties). The structure of a self-assembled oligomers is held together by interactions between 3^1-OH and 13^1-keto groups and the central metal atom (see fig. 1) (Blankenship et al., 1995). In non-polar environment the aggregation is spontaneous. On the other hand, in polar environment BChl *c* remains in a monomeric or a dimeric form. It is possible to distinguish individual forms of BChl *c* by the means of the steady state absorption spectroscopy. The monomeric form has a narrow peak at 668 nm. For the dimeric form this peak is centred at 708 nm. The aggregated form has this peak farther red-shifted depending on the number of molecules participating in the oligomer and their precise interaction. The red-shift of the absorption maxima position is caused by exciton coupling of the pigments (Blankenship et al., 1995). The absorption spectra of individual forms are shown infig. 4. The aggregation in aqueous environment can still be achieved provided that other molecules, like lipids or carotenoids, are added to BChl *c* prior to entering the environment (Klinger et al., 2004). In this case the aggregation is driven by hydrophobic interactions of non polar parts of the molecules. This ability also makes it possible to form artificial antennae with chlorosome-like properties in laboratory.

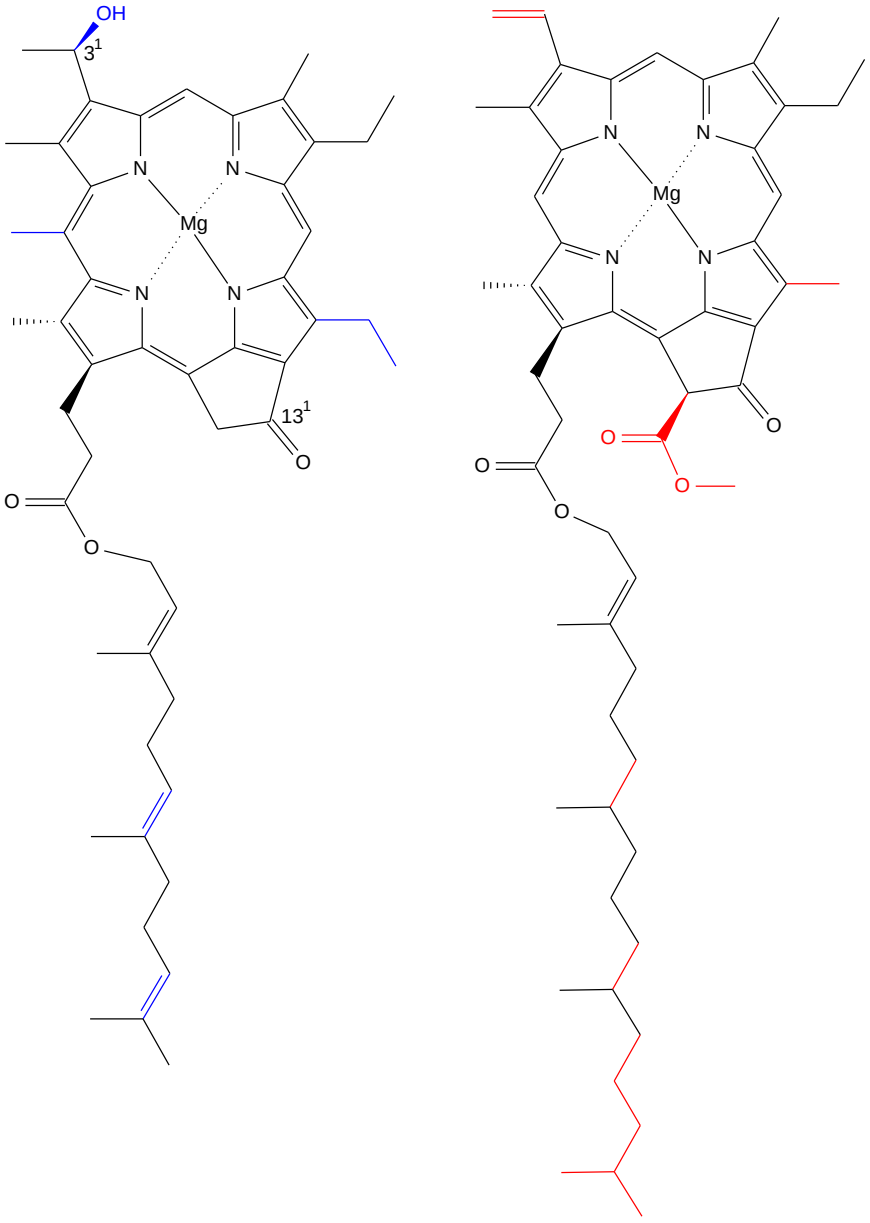

Figure 1: Bacteriochlorophyll c structure (left) and chlorophyll a structure (right). The parts of the molecules that differ are coloured.

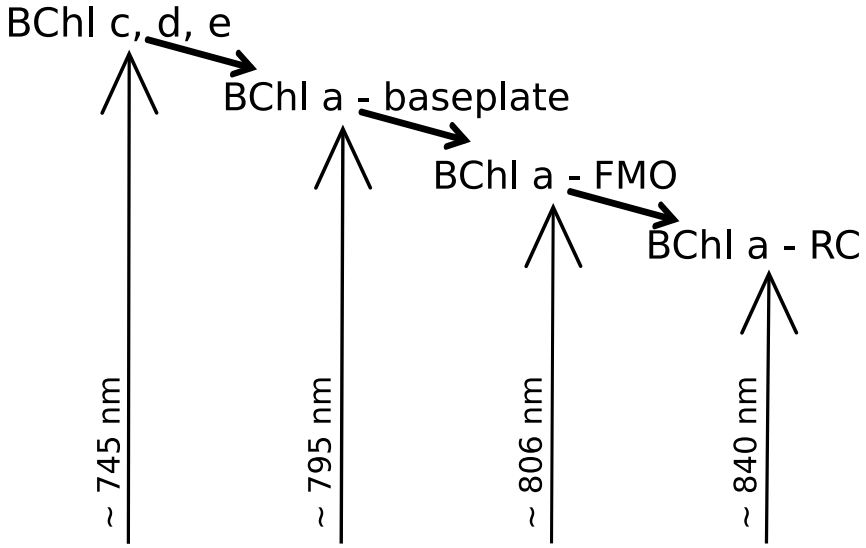

Figure 2: Excitation energy flow schema.

It has been believed that pigments form rod-like elements that fill the chlorosome; recently, Pšenčík et al. (2004) have proposed a lamellar model.

Function of proteins in chlorosomes is largely unknown. The CsmA protein, which forms complex with BChl *a* and carotenoids and provides a channel for the excitation energy transfer from the chlorosome to the so-called Fenna-Matthews-Olson (FMO) complex and further to the reaction centre, is an exception. It is believed that this protein forms a baseplate attaching the chlorosome to the FMO complex. The Q_y absorption band of BChl *a* in the baseplate has a maximum at 795 nm, which is red shifted 25 nm compared to that of the monomeric form of this pigment in methanol, probably due to the pigment-protein interaction, creating a natural "step" for flow of the excitation energy (so-called funnel concept, see fig. 2) (Blankenship and Matsuura, 2003).

Recent results by Vassilieva et al. (2001) indicate that CsmI and CsmJ, and possibly also CsmX, contain FeS centres. The functions of these FeS centres are not yet known, but may possibly relate to the redox regulation of energy transfer in green sulphur bacteria (Blankenship and Matsuura, 2003).

1.2 Excitation energy quenching at aerobic conditions

Green sulphur bacteria are strictly anaerobic organism. They contain type I reaction centres with low-potential electron acceptors. When the bacteria are exposed to air, these acceptors readily react with molecular oxygen, and form a highly reactive activated species such as O_2^- (superoxide) (Frigaard et al., 1997). To prevent destruction of RC, green sulphur bacteria employs a mechanism which dissipates excitation energy in antennae prior to its transfer to RC (and potentially O_2), and effectively lowers concentration of superoxide. Precise nature of this mechanism is unknown, but there are several leads:

- quenching mechanism inside the chlorosomes is activated by a high redox potential (Blankenship et al., 1993)
- efficiency of quenching of steady-state fluorescence depends on the presence or concentration of quinones in chlorosomes or artificial aggregates (Frigaard et al., 1997)
- presence of BChl c^+ was observed in EPR experiments under oxidizing conditions and its involvement in the excitation energy quenching was suggested (van Noort et al., 1997)

In view of these facts several hypotheses have been suggested (Blankenship and Matsuura, 2003). We think that the following is the most likely:

$$\text{BChl } c^*\text{Q} \rightarrow \text{BChl } c^+\text{Q}^- \tag{1}$$

Under oxidized conditions excited antenna's BChl c transfers electron onto quinone (creating probably semiquinone, according to Blankenship et al. (1993) one proton is transferred with electron as well). We expect that the resulting BChl c cation has excited state energy of the first singlet state red-shifted compared to both antenna's aggregated BChl c and baseplate's BChl a, thus acts as a "sink" for excitation energy and prevents its transfer to the reaction centre (see fig. 3). The main aim of this work is to test this hypothesis.

Another redox-dependent excitation energy quenching takes place in FMO complex. Together, both these mechanisms lowers the excitation energy transfer efficiency from nearly 100 % under reducing conditions to approx. 10 % under oxidizing conditions (Blankenship et al., 1993).

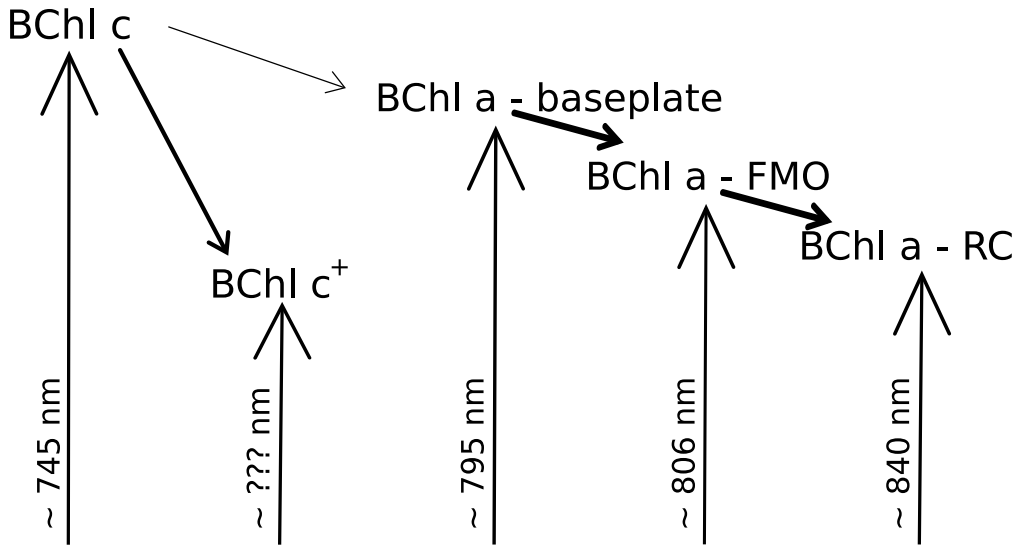

Figure 3: Excitation energy quenching mechanism schema.

2 Samples

We used chlorosomes isolated and pigments extracted from green sulphur bacterium *Chlorobium tepidum*. BChl *c* is the main pigment of this bacteria. The *Chlorobium tepidum* cultures were grown for 3 days at 48 °C in a modified Pfennig's medium (Wahlund et al., 1991) under constant illumination (60 W Tungsten lamp, 25 cm illumination distance). The culture was stored at 4 °C (dark) and whole cells were harvested by centrifugation

2.1 Chlorosomes isolation

The chlorosomes were kindly provided by R. Tuma, University of Helsinki. They were isolated by a method of Gerola and Olson (1986) with modifications. Cell pellets from 250 ml culture were resuspended in 5 ml of 50 mM Tris buffer pH 8, containing 2 M sodium isothiocyanide (NaSCN) and lysed by three passages through a French pressure cell at 20,000 psi. Cell debris was removed by centrifugation. The chlorosome-containing supernatant was loaded onto 10-40 % sucrose density gradient and centrifuged for 24 h at 220,000 g. The chlorosome-containing band was recovered, concentrated by centrifugation, and further purified by another round of density-gradient centrifugation. The density and the optical absorption spectrum of the resulting chlorosomes were measured to assure sample integrity. Chlorosomes were kept frozen till measurement, then dissolved in Tris-HCl buffer.

2.2 Pigments extraction

BChl *c* was extracted from whole cells by means of acetone-methanol 7:2 (vol:vol). The mixture was centrifuged at high speed in a bench centrifuge and the supernatant collected. The pellet was newly suspended in the organic phase. Three cycles were enough to extract quantitatively all pigments. About 1 mM sodium ascorbate was added early to the whole cells to avoid pigment oxidation during the procedure. Phase separation by mixing the extracted pigments with light petroleum-dichloromethane 9:1 (vol:vol) and followed by 1 M NaCl was carried out to bring the bulk of pigments to the non-polar epiphase. Pigments were dried under stream of nitrogen. A first crude separation between BChl *c* (main and secondary homologs) and Car (chlorobactene and its precursors) was achieved by washing out Car from the dried bulky film of pigments by hexane. Pigment fractions enriched in BChl *c* or Car were further purified by reverse phase high-performance liquid chromatography (HPLC) on a Tessek (Prague, Czech Republic) SGX C18 column 8 3 250 mm, particle size 7 μm using solvents A (100 % methanol) and B (methanol-hexane 4:1, vol:vol) in a two-step gradient as follows: 100 % solvent A for the first 10 min and 100 % solvent B for the next 35 min. Each time, the column was (re)equilibrated with solvent A for 15 min before the next injection. The flow rate was 3 mL min^{-1}. The main four homologs of BChl *c* (esterified with farnesol) were collected in one single pool.

2.3 Artificial aggregates preparation

We used lecithine (L-α-phosphatidylcholine, 441601G, Avanti polar-lipids Inc.) instead of MGDG, which is dominant lipid in chlorosome envelope and therefore most often used, as a lipid for BChl *c* aggregates preparation.

The artificial aggregates for experiments were prepared from a mixture of 40 nmol of BChl *c* and 40 nmol of lecithine dissolved in methanol, with addition of various concentrations of quinone vitamin K_1 (95271, Fluka) or vitamin K_2 (V9378, Sigma), injected into 2 ml of vigorously stirred 50 mM Tris-HCl buffer (pH 8). The aggregates without quinones are referred to as pure, the aggregates with quinones are denoted with K_1 or K_2 and quinone to BChl *c* molar ratio. Total volume of organic solvents in sample was under 2.5 %. The aggregates were left for 6 days in dark to fully develop. The formation of aggregates was confirmed by absorption spectroscopy (see fig. 5, compare with fig. 4). It seems that these quinones promotes forming of aggregates similarly to Car as reported in (Klinger et al., 2004). In support of this fact we have successfully formed aggregates using only BChl *c* and K_1 (spectra not shown). Interestingly, for K_1 in molar concentration to BChl *c* 1:1 the position of Q_y absorption maximum was blue-shifted compared to that of aggregates without quinones, whereas total absorption increased, and monomer concentration decreased. It suggests that more BChl *c* molecules were incorporated into aggregates, but these aggregates were either smaller or, more likely, that the short distance interactions of BChl *c* molecules within aggregate were modified. Aggregates were kept in Tris-HCl buffer in dark at 5-8 °C.

In addition, samples with several different concentrations of BChl *c* and lecithine were prepared in order to find out the influence of lecithine concentration upon aggregation. Absorption spectra of these samples are shown in fig. 6. These spectra were also measured 6 days after samples preparation to ensure the aggregates were fully developed. Again the peaks at 668 nm arise from absorption of monomeric BChl *c*, the peaks beyond 715 nm correspond to absorption of aggregated BChl *c*. The spectra were normalized at monomeric form absorption and ratio of absorption of aggregated form to absorption of monomeric form was computed (see table 1).

The absorption maximum position is least red-shifted for low lecithine concentration ratios (1:0.2 or 1:0.5, BChl *c*:lec mol:mol) indicating that the aggregates are too small. The highest aggregated to monomeric form ratio accompanied with the largest red-shift was achieved for concentration ratio 1:1 and 1:2. An overall absorption tends to decrease with an increasing concentration of lecithine. Interestingly, the absolute absorption of monomeric form increases significantly for higher concentrations of lecithine. Since BChl *c* is not soluble in aqueous buffers in a monomeric form (see fig. 4), the results probably indicate formation of one BChl *c* molecule containing micelles protecting BChl *c* from precipitation on the cuvette surface. Even if the monomeric to aggregated form ratio is not favourable, the area of concentration ratios around 1:7 could prove useful for aggregate preparation, because most BChl *c* molecules seem to be incorporated into aggregate at this lecithine concentration.

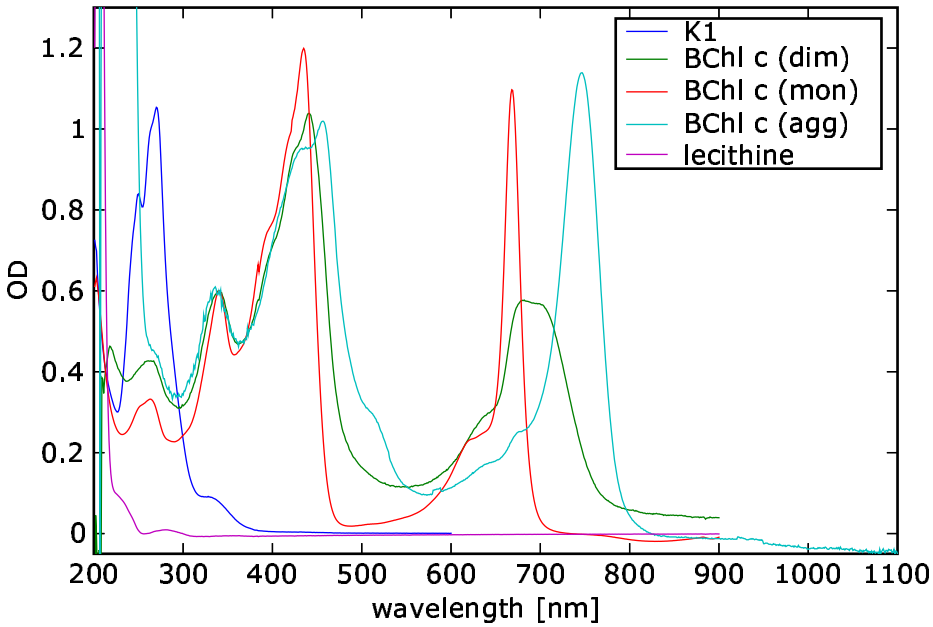

Figure 4: Steady state absorption spectra of BChl *c* dissolved in methanol (monomeric form), BChl *c* in aqueous buffer (dimeric form), chlorosomes (BChl *c* aggregated form), lecithine in methanol and K_1 in methanol (15 μM). The spectra of BChl *c*forms were aligned at 340 nm.

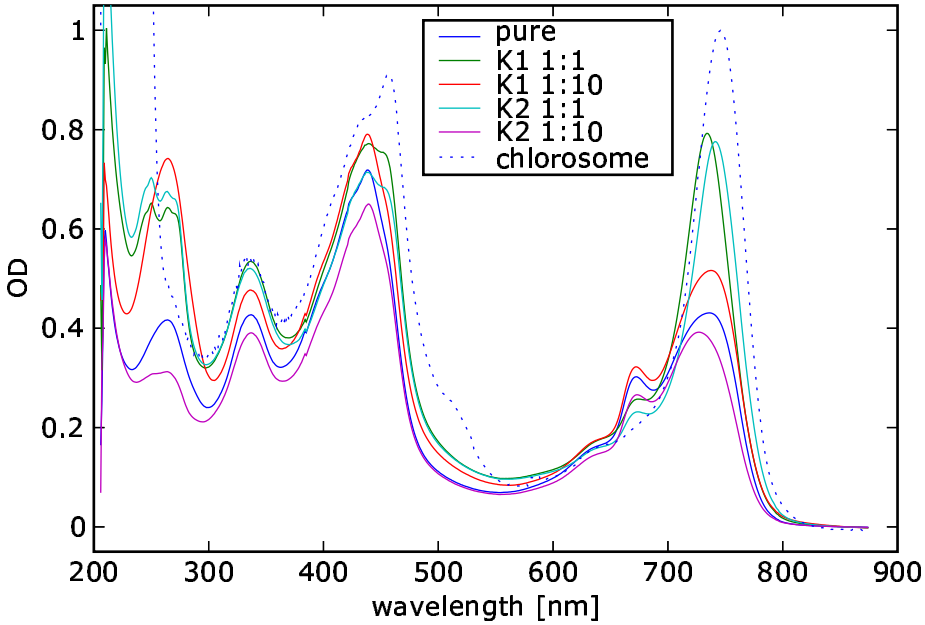

Figure 5: Steady state absorption spectra of artificial aggregates used in experiments. For composition of individual samples see sec. 2.3. Steady state absorption of chlorosomes is included for sake of comparison.

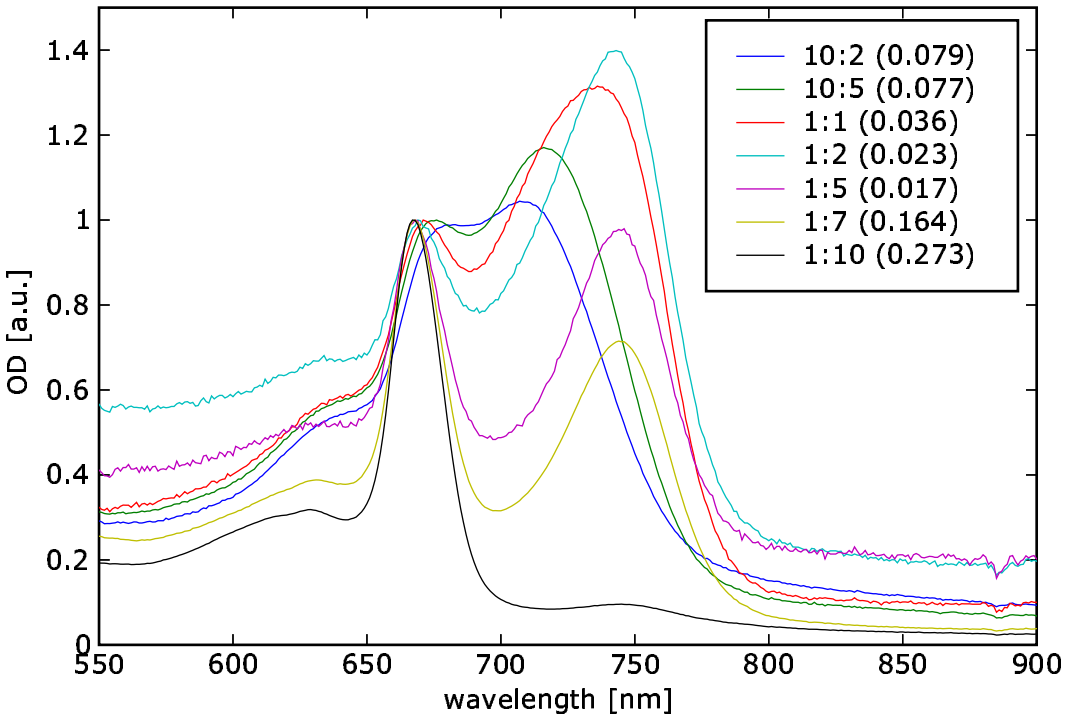

Figure 6: Absorption spectra of artificial BChl *c*-lecithine aggregates with several different relative concentrations. The spectra were normalized to unity at the maximum of monomeric BChl *c* form absorption for sake of comparison. The legend shows BChl *c*:lecithine mol:mol ratio and, in parenthesis, the real amplitude of monomeric BChl *c* form absorption.

Table 1: Absorption maxima positions and ratios between monomeric and aggregated form of BChl *c* in artificial BChl *c*-lecithine aggregates for several relative concentrations.

BChl:lec [mol:mol]	λ_{mon} [nm]	λ_{aggr} [nm]	A_{aggr}/A_{mon}
10:2	695	707	1.04
10:5	676	716	1.17
1:1	671	736	1.32
1:2	669	743	1.40
1:5	668	746	0.98
1:7	668	744	0.71
1:10	667	696	0.13

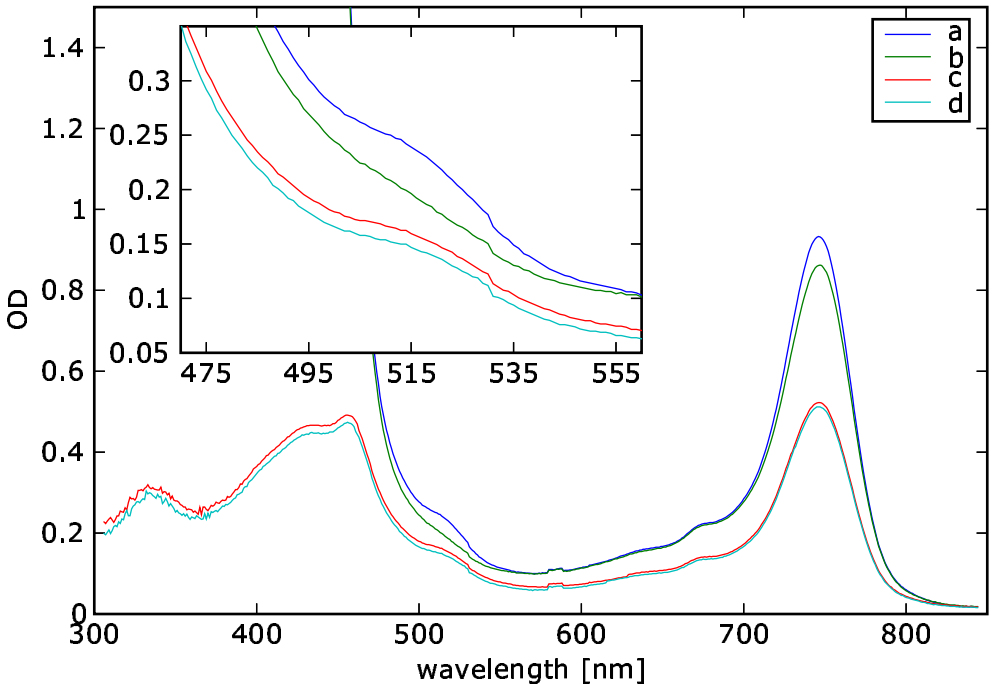

Figure 7: Steady state absorption spectra of FCN chlorosomes (prior - a - and after - b - measurement) and normal chlorosomes (prior - c - and after - d - measurement). The inset shows Car absorption region in detail.

Samples were measured under several different redox conditions:

- without any redox mediators added and freely accessible to air oxygen, referred to as "normal", redox potential of buffer $350 \pm 30\,\mathrm{mV}_H$
- with addition of 2-4 mM potassium ferricyanide ($K_3[Fe(CN)_6]$) to enhance oxidized-condition effects, referenced as "FCN", redox potential of buffer $540 \pm 30\,\mathrm{mV}_H$
- with addition of 11 mM sodium dithionite ($Na_2O_4S_2$) (incubated in dark in sealed cuvettes for 0.5-1 hour after addition) to form reducing conditions, referenced as "Dit", redox potential of buffer $-443 \pm 30\,\mathrm{mV}_H$ (redox potential measurement was conducted in an open cuvette, therefore the value may slightly differ from true redox potential in a sealed cuvette)

Integrity of samples was checked by steady state absorption spectroscopy before and after measurements. The effect of measurement on normal or Dit samples was small decrease of absorption, probably caused by precipitation of antennae on cuvette walls. Addition of $K_3[Fe(CN)_6]$ resulted in noticeably larger decrease of both BChl *c* and Car absorption. This effect was not caused by measurement (as tested by control sample), but by $K_3[Fe(CN)_6]$ itself. Similar effect has been observed by Valentin et al. (2002). Experiments were conducted at room temperature.

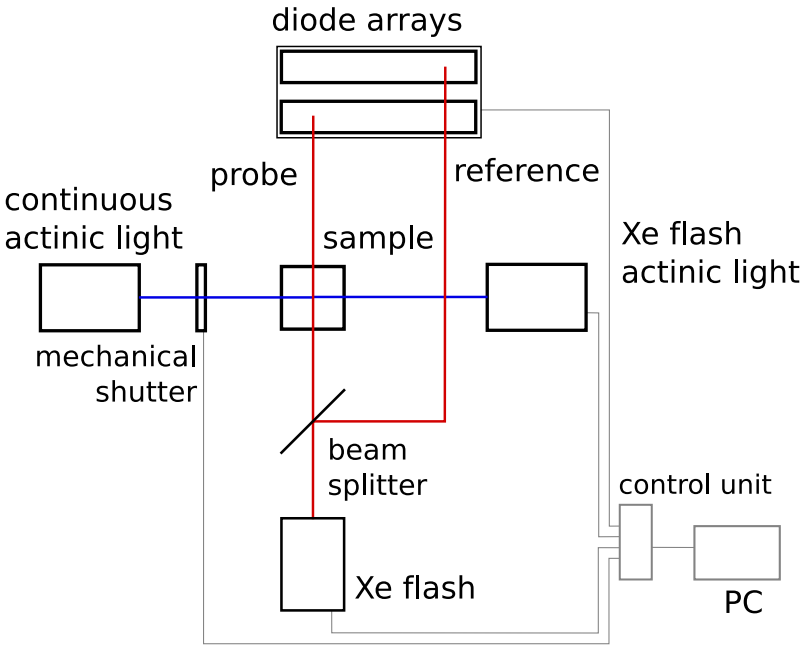

Figure 8: Schema of the apparatus used for difference absorption spectroscopy measurement. Individual components are described in text.

3 Apparatus

3.1 Transient absorption spectroscopy

We measured the difference of absorption spectra of the sample induced by illumination. The schema of used apparatus is shown in fig. 8. Transient changes in the sample could be induced by two different sources of actinic light: Xe flash lamp (FX249, $EG_{\Sigma}G$) with a pulse length 1.3 μs and an energy in a pulse 4 mJ, used in measurement of triplet-minus-singlet (TmS) spectra with microsecond resolution; or continuous halogen light (21 V, 150 W, Osram) with radiative flux at sample 850–1700 $\mathrm{mE\,m^{-2}s^{-1}}$ (the magnitude of induced changes in the sample was not significantly dependent on the intensity of the actinic light in this range), controlled by the mechanical shutter with response time $\sim$ 0.5 ms, used in measurement of transient absorption spectra evolution for spans in range from seconds to minutes. The sample was probed by Xe-flash lamp (FX1161, $EG_{\Sigma}G$) with a pulse length 0.9 μs and an energy in a pulse 2-15 μJ (at the sample place) depending on a used filter; filters were chosen to ensure optimal signal intensity on the detector. Two diode arrays (2×36 diodes) connected to MS 257 polychromator (Oriel Instruments) were used as a detector for probe and reference. Individual components were synchronized by a programmable control unit connected to PC.

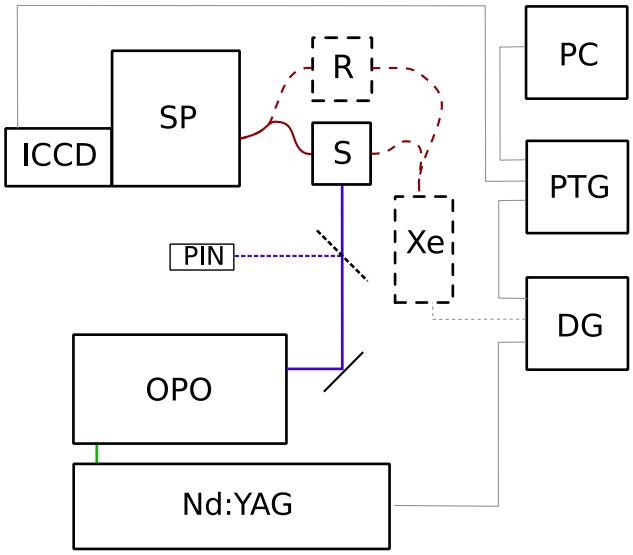

Figure 9: Fluorescence spectroscopy apparatus schema. Individual components are described in text. Only a part of more versatile apparatus was used; the dashed components were not utilised.

3.2 Fluorescence spectroscopy

Experimental set-up for measuring fluorescence spectroscopy is shown in fig. 9. The sample (S) was excited with pulses (460 nm, 0.45 ± 0.03 mJ in 5 ns pulse) generated by the optical parametric oscillator (OPO) (PG 122/SH, EKSPLA) pumped by the third harmonic of the Nd:YAG laser (NL 3036, EKSPLA). Fluorescence was collected by a collimator and led by an optical fibre to the spectrograph (TRIAX 320, HORIBA Jobin Yvon, grating 100 gr/mm, blaze 450 nm, SP). The signal was detected by intensified CCD camera (PI-MAX 512RB, 512×512 chip, Roper Scientific, ICCD). Individual components were synchronized by the programmable timing generator (PTG) coupled with the delay generator (DG). The data were collected by the PC.

3.3 Subsidiary instruments

Since the experiments took place in several laboratories we used three different spectroscopes for measuring steady state absorption spectra of samples: UV-300 (Spectronic Unicam), UV/VIS Lambda12 (Perkin Elmer) and AvaSpec-1024-SPU (Avantes). We used combined redox/pH-meter GMH 3530 (GREISIMGER electronic GmbH) with electrodes GE 105 and GE 100BNC for measuring of redox potential and pH, respectively.

4 Measurements

4.1 Transient absorption spectroscopy

TmS spectra of chlorosomes and artificial aggregates were measured with the apparatus described in sec. 3.1. Delay between excitation and probe pulse was in range 0.5 μs-100 ms. Since the signal intensity was close to detection limit of the apparatus, the signal to noise ratio is rather low. Only distinguishable signal was for FCN chlorosomes at 543 nm with $< 0.5\,\mu$s raise and 10 μs fall which is connected to Car triplets (see figures 10 and 11). There were also observed negative peaks at 750 nm and 450 nm but these showed no evolution on this time scale. Because we were interested in signal from the anticipated BChl *c* cation in near infrared region with amplitude an order of magnitude weaker than that at 750 nm, we decided to measure transient absorption with the continuous actinic light, expecting stronger signal due to the accumulation of the light induced change product.

Even though the product accumulation helped, some of the spectra, especially those acquired for short times of actinic light exposures, were still noisy. Therefore, we tried to remove noise computationally.

4.1.1 Spectra smoothing

Attempts to clean the spectra using moving average were unsuccessful, because this procedure lowers maxima of peaks significantly. Considering the fact that the observed signal formed peaks distributed over several diodes, whereas the most prominent noise was in the form of one diode spikes, we decided to remove it by filtering out high frequencies of Fourier transform of the signal. The typical noisy spectrum, the result of this procedure and comparison with moving average is shown in fig. 12. We used *Fastest Fourier Transform in the West* library (Frigo and Johnson, 2005) implemented in SciPy (Jones et al., 2001) for computing fast Fourier transform.

Since individual diodes had slightly different dark signal, which affects low intensity signal (OD $\sim 10^{-4}$), the first few spectra of each time series were measured without actinic light and their average served as background for given wavelength. All transient absorption spectra were corrected in this way unless mentioned in the text. This procedure could not be used for TmS spectra, because they were measured for one time delay at a time. It should be noted that as far as the time evolution of the sample at one wavelength is concerned this procedure is ancillary because it reduces to adding a constant.

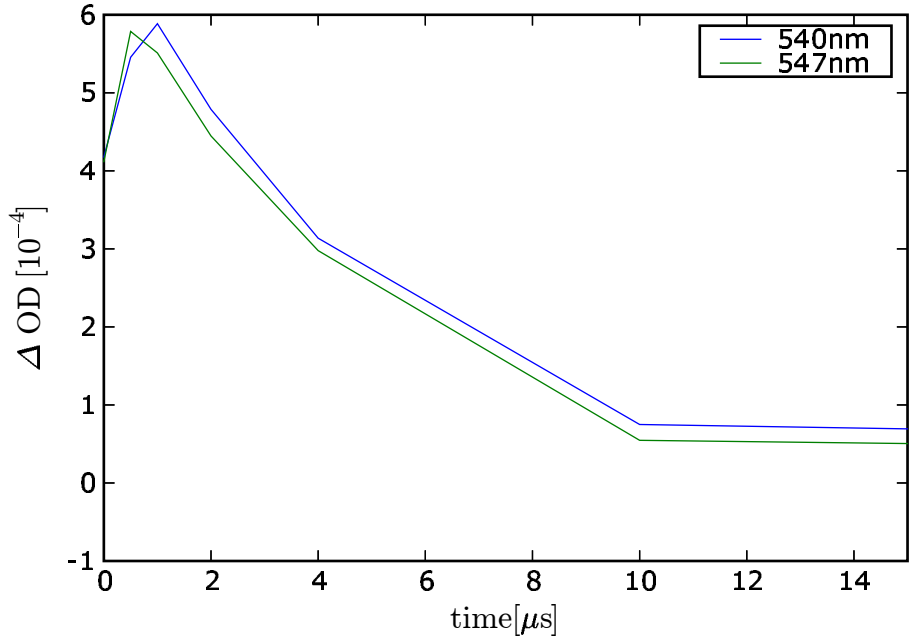

Figure 10: FCN chlorosomes TmS kinetics.

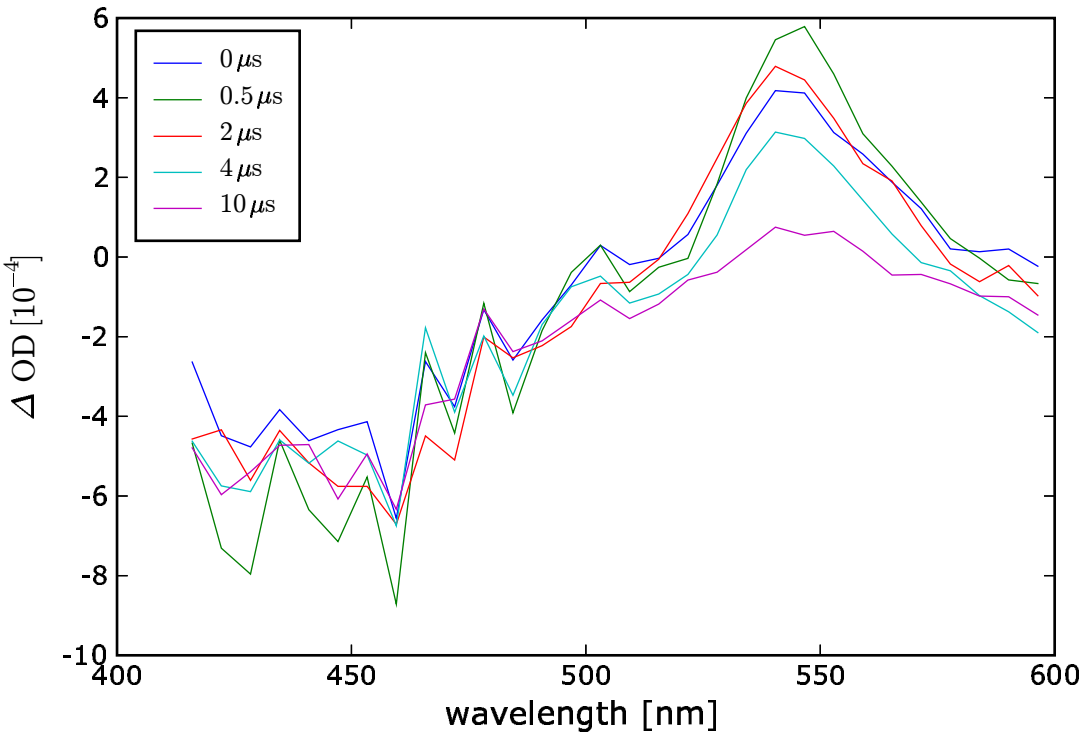

Figure 11: FCN chlorosomes TmS spectra. Times in legend denote delay between exciting and probing pulse.

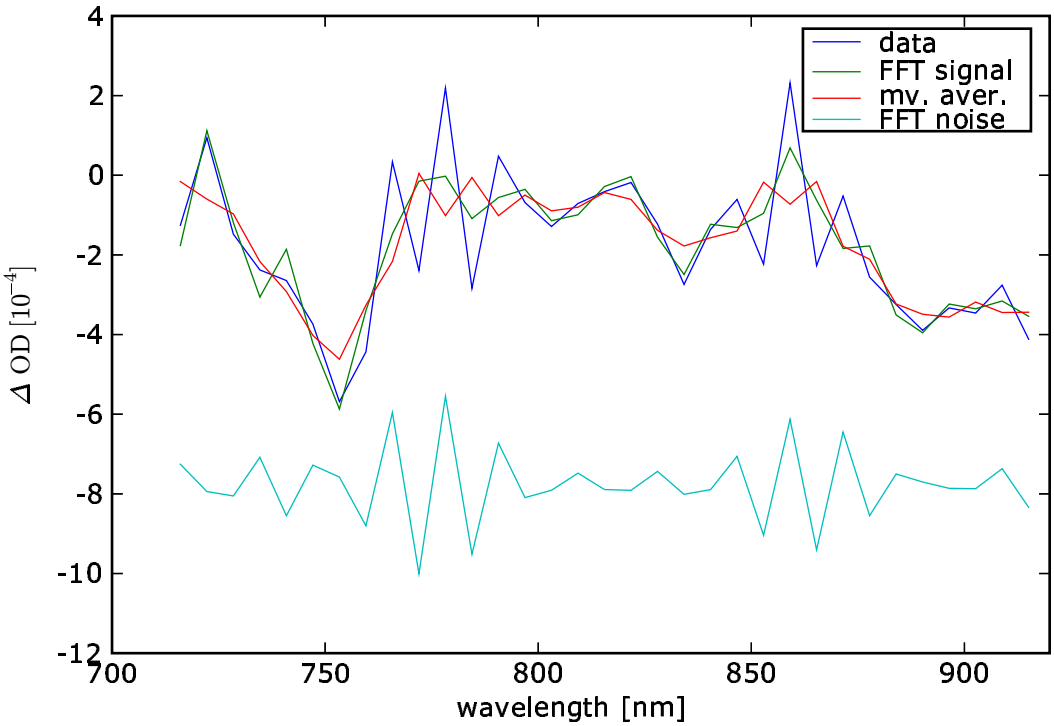

Figure 12: Smoothing methods comparison. The original noisy spectrum is denoted as "data". The spectrum was cleaned by moving average ("mv. aver.") and by fast Fourier transform ("FFT signal"). Part of the signal identified as a noise by fast Fourier transform is also shown ("FFT noise"). These data were not corrected for dark signal as described in sec. 4.1.1

4.1.2 Processed spectra

The continuous actinic light transient absorption experiments were conducted only for chlorosome samples. Processed spectra are shown in figures 13 and 14. They are combined from five and three, respectively, fft-cleaned spectra across the whole (measured) spectral range. The neighbouring spectra were measured in a way to have sufficiently large spectral overlaps to enable glueing of the spectra. The spectra were averaged in overlapped parts.

Let us first analyse the transient absorption spectrum of normal chlorosomes, which has been measured over wide wavelength range. The negative peaks at 750 nm and 450 nm correspond to the decrease of the BChl *c* aggregates Q_y and Soret band absorption, respectively. The negative band at 600–700 nm can also be ascribed to the decrease of the BChl *c* aggregates absorption. The negative peak at 510 nm arises from the decrease of Car absorption. Comparison with inverted steady state absorption of the sample reveals two interesting facts. Firstly, the peak at 750 nm is narrower and slightly red-shifted to Q_y absorption, indicating that process responsible for this peak occurs after fast exciton relaxation from the higher excitonic states of BChl *c* (with absorption maximum at 750 nm), which possess the main oscillator strength, to the lowest excited state of BChl *c* (with absorption maximum farther to red) and that mainly these states undergo change (Pšenčík et al., 2003). Secondly, the decrease at 450 nm is shallower than what should be expected from proportions of steady state absorption at Q_y and Soret band maxima. It seems that there is another component in this region with a positive amplitude (at 84 s approx. $10 \cdot 10^{-4}$ at 450 nm). The shape of spectra suggests that the peak of this component is located below 450 nm (the positive component dominates at the blue end of the spectra, nevertheless this can be due to some artefact). The positive band at 520–550 nm can probably also be assigned to this component.

The others major features are the broad positive peak around 960 nm and the broad positive band at 800–900 nm. There is also a clearly identifiable positive peak in aggregated BChl *c* 600-700 nm negative band centred at $\sim$ 700 nm. The last distinguishable feature is the peak at 560 nm. These positive components arise from increasing absorption of products of light induced changes. They are further analysed in discussion (sec. 5.1).

The FCN sample spectrum is comparable to normal sample spectrum. The only difference (aside from bigger amplitude of the signal) is missing peak at 820 nm.

Time development of the decrease at 750 nm for several lengths of actinic light exposure is shown in fig. 15. It is evident that kinetics has at least two components: one exponential; the other almost linear. It can also be seen that relaxation in dark is slower than reaction to actinic light. The data indicates that amplitude of the exponential component is always the same and that this component is fully reversible during the span of experiment, that implies lifetime < 2 s, whereas the linear component is reversible only partially during the span of the experiment.

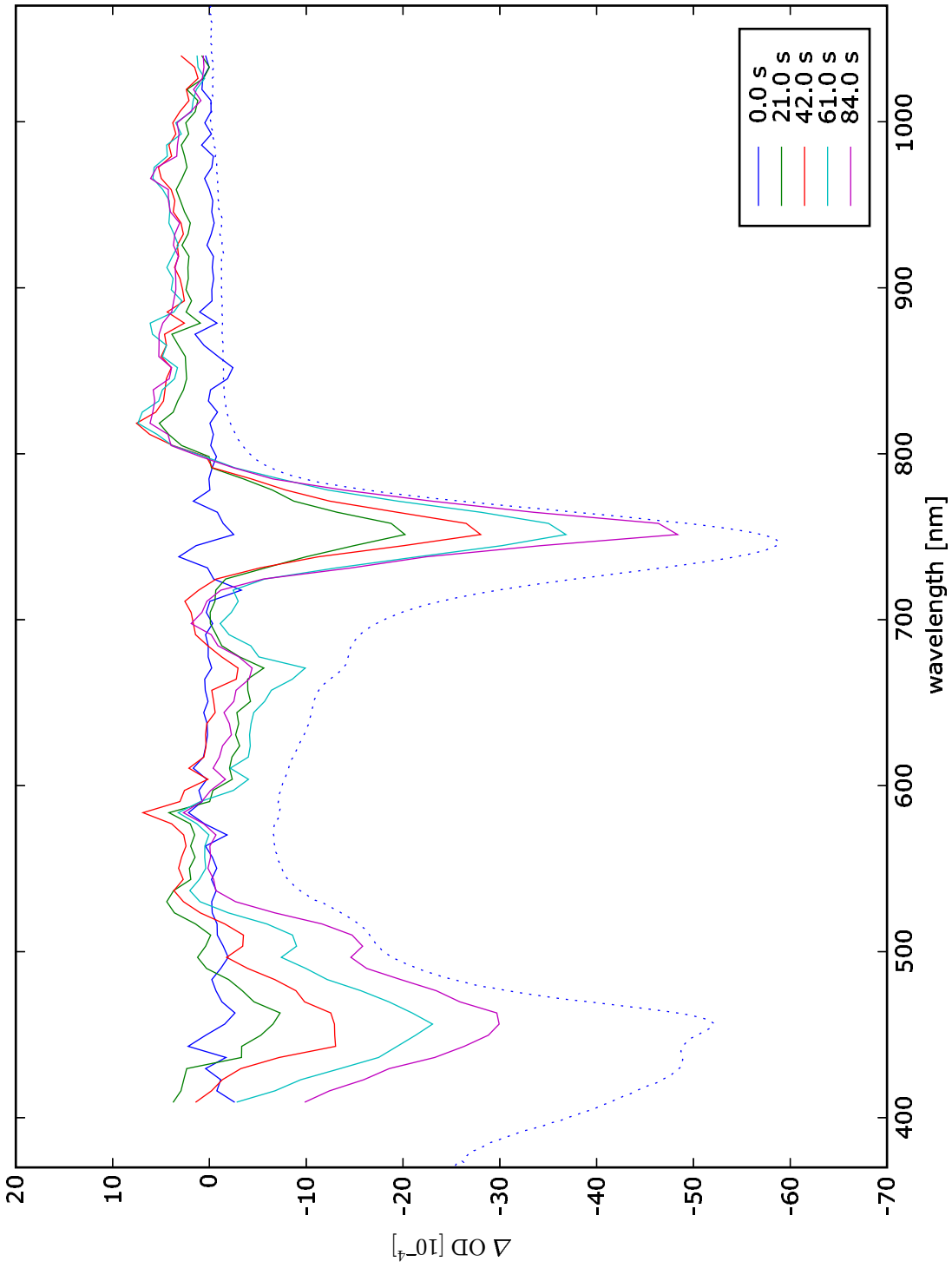

Figure 13: Processed transient difference absorption spectra of normal chlorosomes. The times in legend denotes time elapsed since turning on the actinic light. The actinic light exposure lasted for 80 s. The dashed line represents negated steady state absorption spectrum of the sample before the measurement (real absorbance at Q_y band was 1.2).

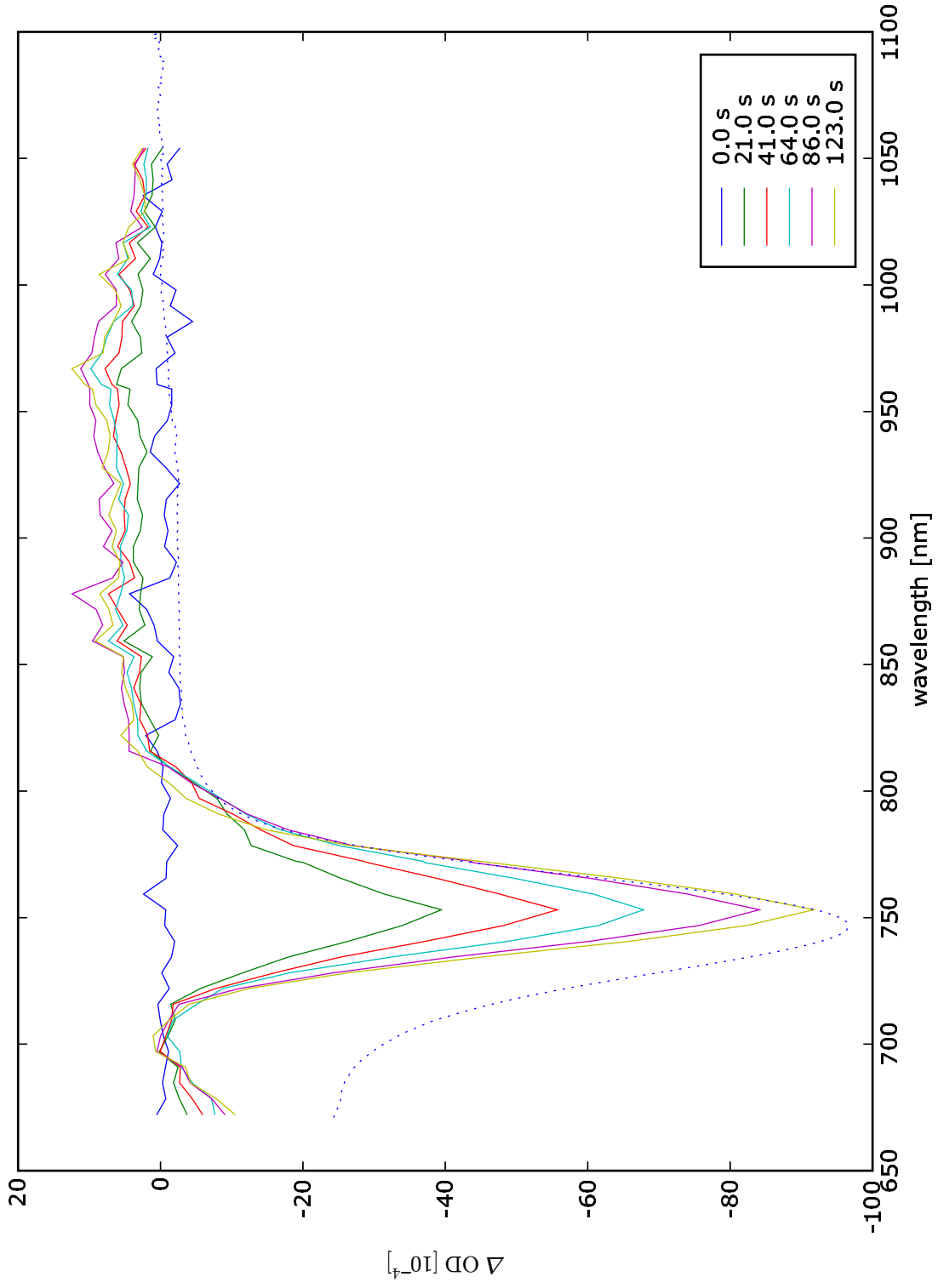

Figure 14: Processed transient difference absorption spectra of FCN sample. The times in legend denotes time elapsed since turning on the actinic light. The actinic light exposure lasted for 115 s. The dashed line represents negated steady state absorption spectrum of the sample before the measurement (real absorbance at Q_y band was 1).

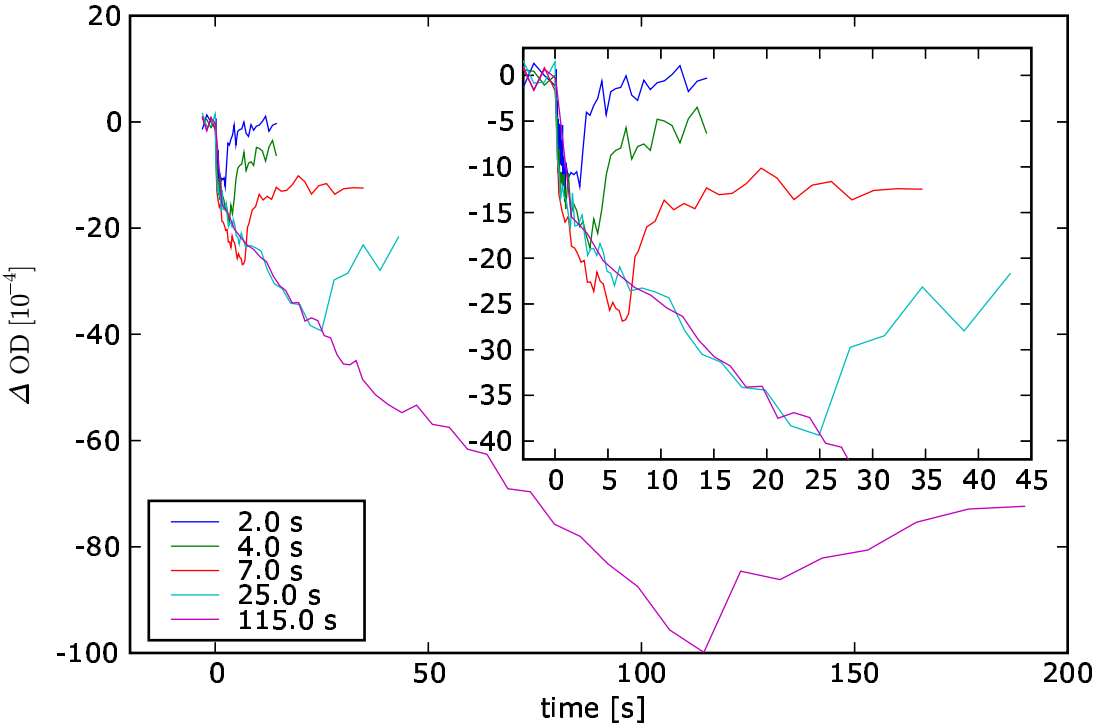

Figure 15: Kinetics of light induced changes in FCN chlorosomes at 750 nm. The times in legend denotes length of actinic light exposure.

4.1.3 Kinetic models

We tried to describe the time development of the spectra with monoexponential decay

$$A_0 + A_1\, exp(-\frac{t}{T_1}), \tag{2}$$

but, as expected, it did not fit the data sufficiently. Biexponential decay

$$A_0 + A_1\, exp(-\frac{t}{T_1}) + A_2\, exp(-\frac{t}{T_2}) \tag{3}$$

reflected the evolution more precisely. For longer actinic light exposures the longer lifetime component tended to grow to infinity, which implies that it is much longer than the duration of experiment. The last function used to fit the data, linear-exponential model, takes advantage of this fact:

$$A_0 + A_1\, t + A_2\, exp(-\frac{t}{T_2}). \tag{4}$$

The linear-exponential model fits the data equally well as biexponential model for long actinic light exposures as can be seen from comparison plots (figures 16–18). For shorter times of actinic light exposure the biexponential model fits the data better, probably because it has one more degree of freedom, but the linear-exponential model describes the overall trend, which we are interested in, well enough. As far as the physical interpretation of the linear-exponential model is concerned, the exponential part may represent electron transfer over short distances, with finite number of electron acceptor available, possibly inside chlorosome, while linear component may represent transport over longer distances, with "infinite" number of electron acceptors available, possibly outside of chlorosome.

The data were fitted by linear-exponential model using a modification of the Levenberg-Marquardt algorithm implemented in SciPy (Jones et al., 2001). Standard deviations of fitted parameters were computed as square roots of diagonal elements of the estimate of the covariance matrix. It should be noted that control unit of transient absorption apparatus supported only limited number of time steps in one time series, and we decided to concentrate on the actinic light induced kinetics. Therefore, relaxation kinetics, and especially their exponential part, were not sampled densely enough to determine A_5 and T_5 as precisely as their AC kinetics counterparts (we used the same model for both parts of kinetic with A_0, A_1, A_2, T_2 standing for parameters of the actinic light part and A_3, A_4, A_5, T_5 standing for parameters of dark part).

Figure 16: Models comparison for long actinic light exposures. For models definition see sec. 4.1.3. The number in parenthesis is the sum of the squared differences.

Figure 17: Models comparison for middle actinic light exposures. For models definition see sec. 4.1.3. The number in parenthesis is the sum of the squared differences.

Figure 18: Models comparison for short actinic light exposures. For models definition see sec. 4.1.3. The number in parenthesis is the sum of the squared differences.

Table 2: Parameters of kinetics of light induced changes in FCN chlorosomes at 750 nm for several different times of actinic light exposure (AC time). Overall absorbance difference for AC part of experiment and for subsequent dark relaxation and parameters of exponential component of model are shown.

	AC			dark		
AC time	ΔOD $[10^{-4}]$	$\lvert A_2 \rvert$ $[10^{-4}]$	T_2 [s]	ΔOD $[10^{-4}]$	$\lvert A_5 \rvert$ $[10^{-4}]$	T_5 [s]
2s	-10.0(100)	13.3(48)	0.54(22)	9.1(73)	8.8(9)	1.47(27)
4s	-17.4(12)	10.9(8)	0.23(3)	12.1(21)	8.3(12)	1.46(32)
7s	-23.2(64)	15.6(27)	0.42(11)	13.7(29)	10.8(43)	1.17(22)
25s	-38.9(3)	13.6(18)	0.32(3)	17.2(22)	9.5(15)	1.44(65)
115s	-92.2(5)	18.4(20)	3.96(34)	26.0(21)		

4.1.4 Kinetics

Parameters of the kinetics shown in fig. 15 were determined using the linear-exponential model. They are summarized in table 2. The results are in agreement with observations made in sec. 4.1.2. The exponential components are independent on the length of actinic light exposure (the values for 115 s are misleading; the exponential component was not sampled densely enough in this measurement), whereas overall absorption difference grows for longer exposures. The lifetime of exponential component for actinic light part (~ 0.4 s) is shorter than the lifetime for dark part (~ 1.3 s). The exponential component seems to be almost reversible with amplitudes $\sim 13 \cdot 10^{-4}$ and $\sim 10 \cdot 10^{-4}$ for actinic light part and dark part, respectively.

Exemplary kinetics for individual samples at 750 nm, 850 nm and 960 nm are shown in figures 19–21. The wavelengths were chosen so as to map the major decrease of BChl *c* aggregate absorption and the major increase of developing products. Fitted parameters averaged over all conducted measurements and neighbouring wavelengths are summarized in appendix A. It is evident that signal amplitude depends on redox potential. Addition of $K_3[Fe(CN)_6]$increases signal amplitude approximately twofold compared to normal sample, whereas addition of sodium dithionite diminished signal so much that exponential part of the model could not be fitted. The kinetics are discussed more deeply in sec. 5.2.

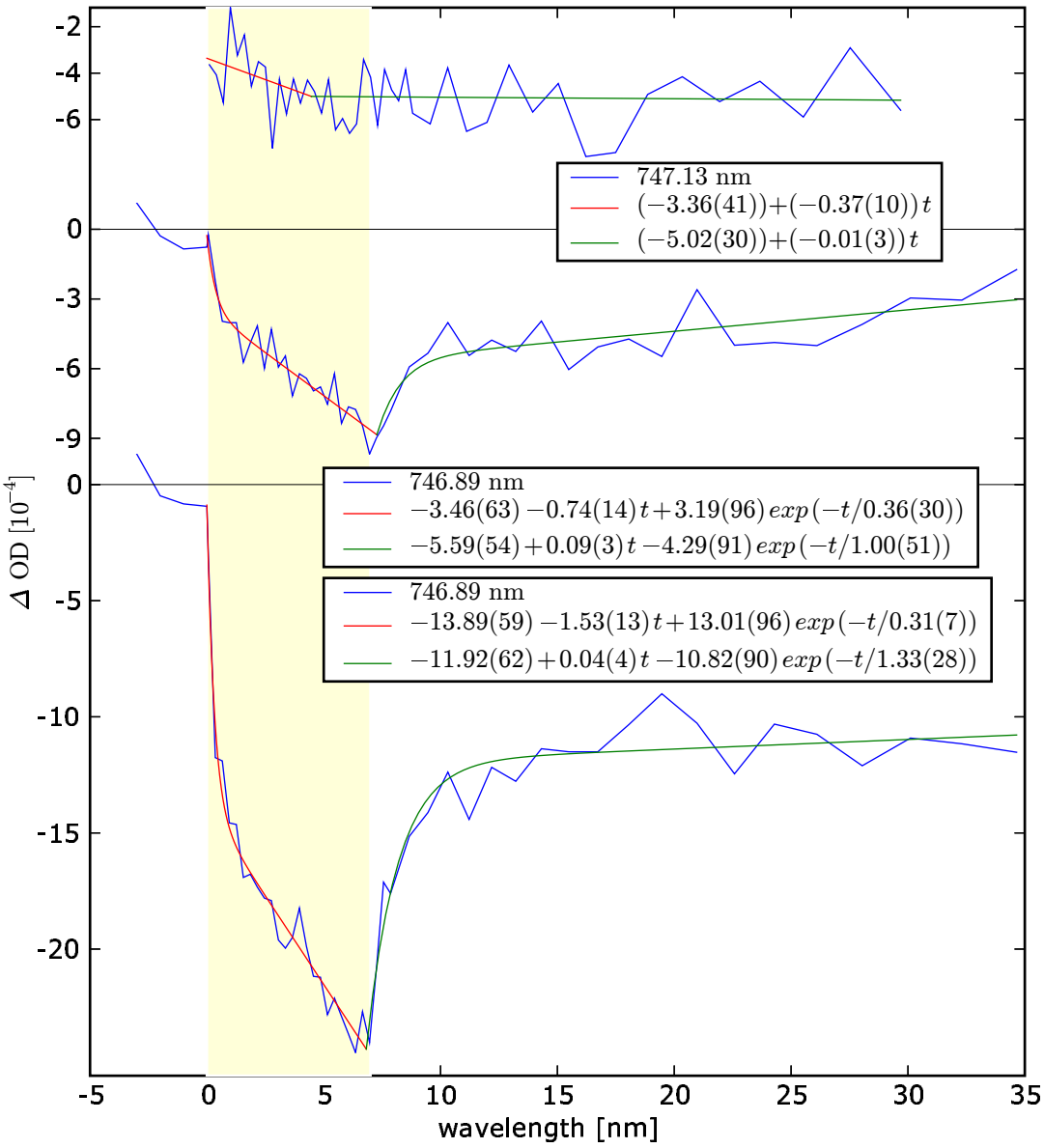

Figure 19: Kinetics at $\sim$ 750 nm for (from top to bottom) Dit(OD 0.5, aver. 3), normal(OD 0.5, aver. 3), FCN(OD 1). In parenthesis are listed maximum steady state absorbance of the sample at Q_y band before the measurement and optionally a number of measurements over which is the kinetic averaged. The legends show wavelength and parameters (with error) corresponding to eq. 4 (if exponential component could not be determined, only linear component is shown). Yellow background indicates actinic light on.

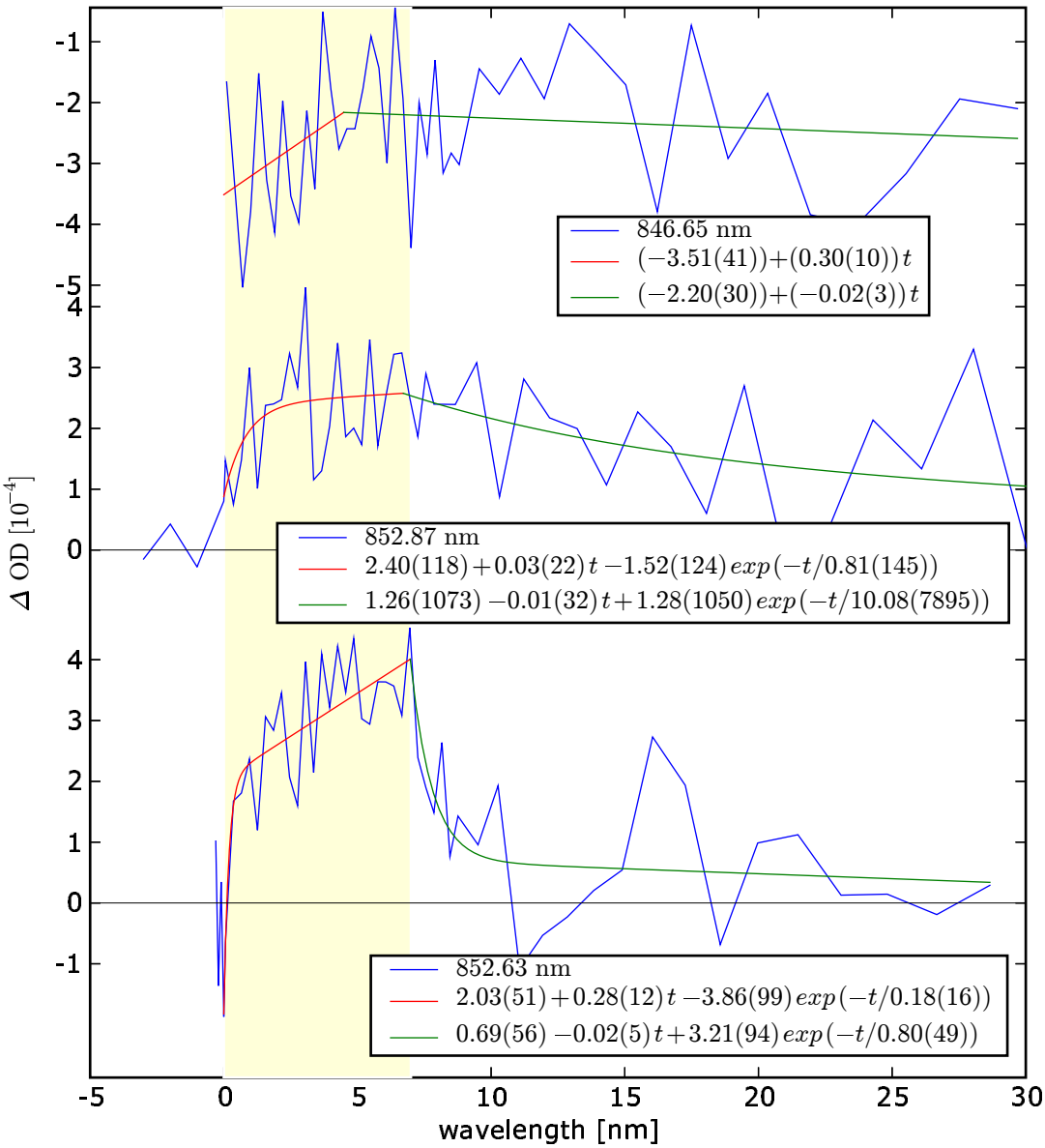

Figure 20: Kinetics at $\sim$ 850 nm for (from top to bottom) Dit(OD 0.8, aver. 2), normal(OD 0.8, aver. 4), FCN(OD 1). In parenthesis are listed maximum steady state absorbance of the sample at Q_y band before the measurement and optionally a number of measurements over which is the kinetic averaged. The legends show wavelength and parameters (with error) corresponding to eq. 4 (if exponential component could not be determined, only linear component is shown). Yellow background indicates actinic light on.

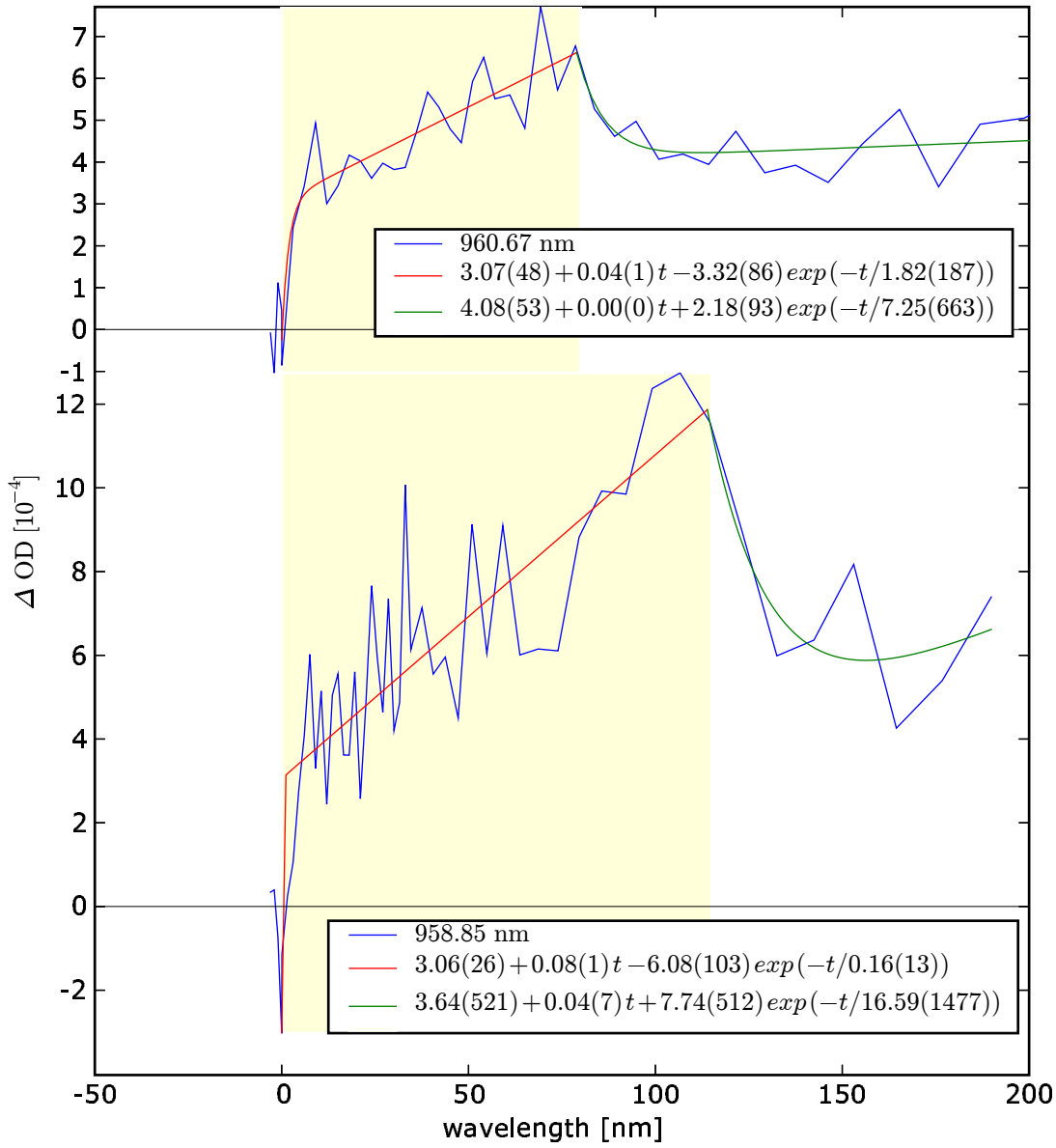

Figure 21: Kinetics at ~ 960 nm for (from top to bottom) normal(OD 1.2, aver. 2), FCN(OD 1). In parenthesis are listed maximum steady state absorbance of the sample at Q_y band before the measurement and optionally a number of measurements over which is the kinetic averaged. The legends show wavelength and parameters (with error) corresponding to eq. 4. Yellow background indicates actinic light on.

4.2 Fluorescence spectroscopy

In order to determine whether the excitation energy quenching at aerobic conditions takes place also in artificial antenna and to study the role of quinones, the fluorescence spectra of artificial aggregates with and without incorporated quinones were measured at aerobic conditions. Then a reducing agent was added and measurement was repeated. Apparatus described in sec. 3.2 was used. The spectra are shown in figures 22–24. It is apparent that fluorescence intensity is higher at reducing conditions and consequently that excitation energy is quenched at aerobic conditions. The quenching is significantly enhanced in aggregates containing quinones. Acquired results are summarized in table 3 and discussed in sec. 5.3.

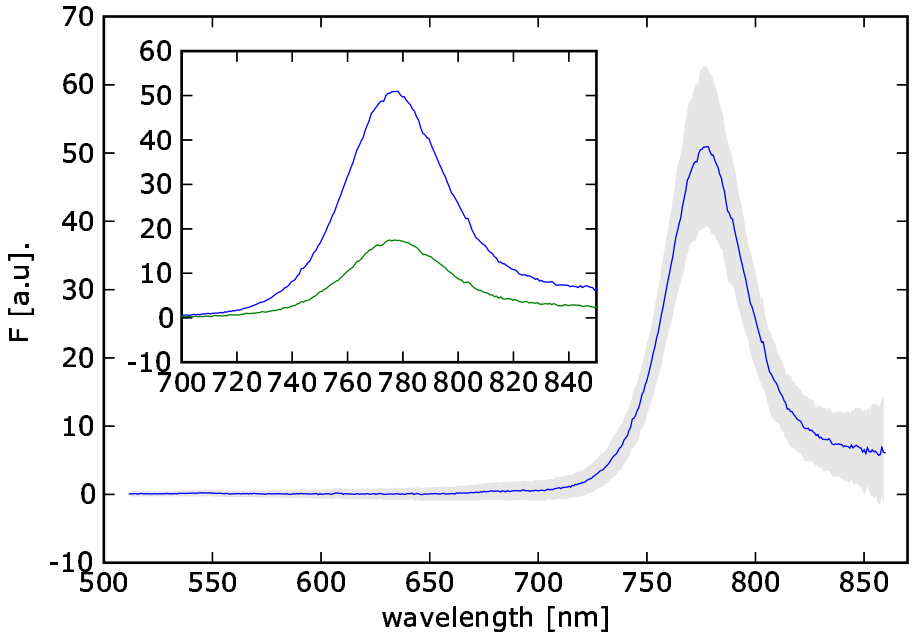

Figure 22: Fluorescence spectra of pure BChl *c* aggregates.

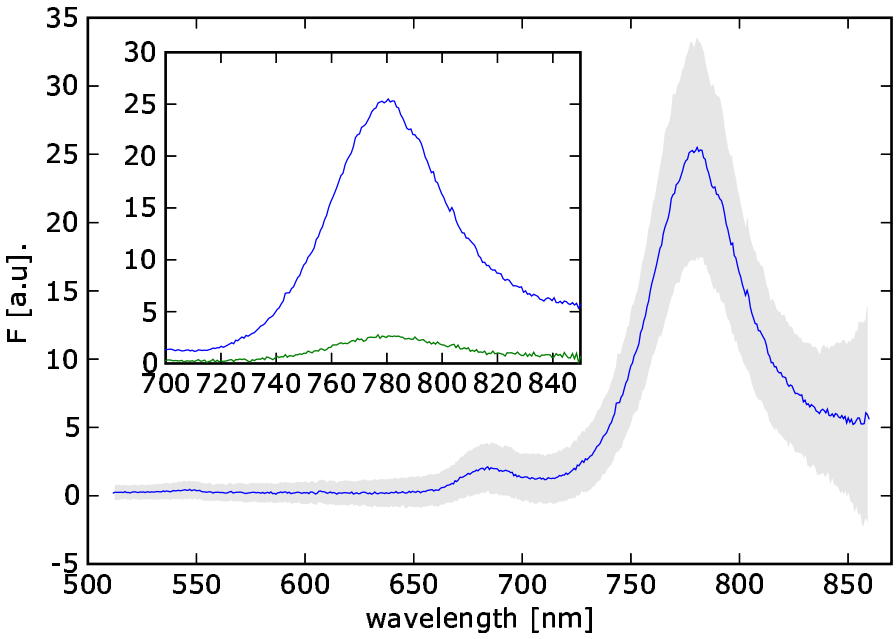

Figure 23: Fluorescence spectra of aggregates with K_1 1:1.

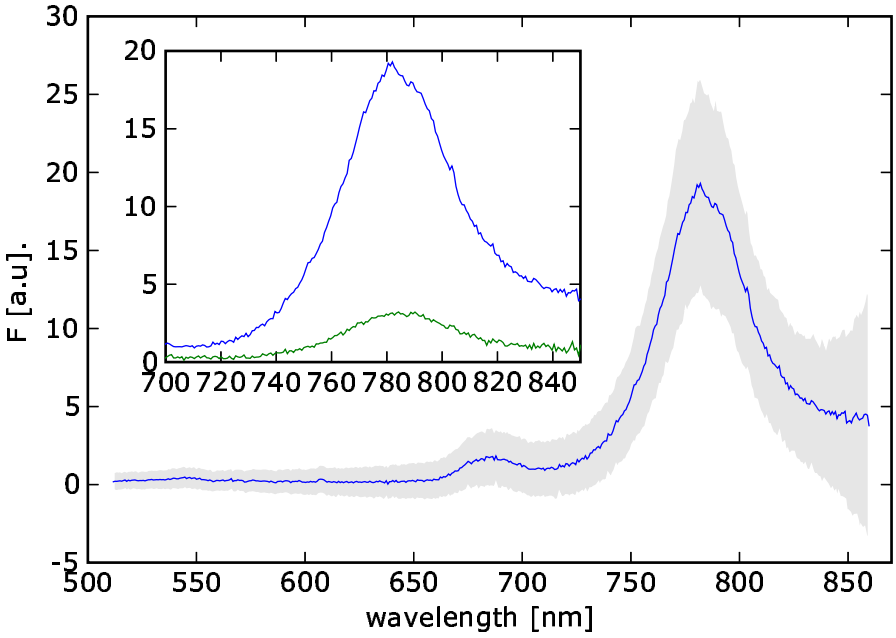

Figure 24: Fluorescence spectra of aggregates with K_2 1:1.

Table 3: Fluorescence maxima positions, relative fluorescence intensity at aerobic and reducing conditions and the ratio of reducing to aerobic relative fluorescence intensity. In parenthesis is quinone:BChl *c* molar ratio of sample. Values for detergent treated chlorosomes (these chlorosomes do not contain proteins in their lipid layer) and for BChl *c* aggregates containing chlorobiumquinone are shown for sake of comparison.

aggregates	λ_{max} [nm]	F_{ox}/A_{Q_y}	F_{red}/A_{Q_y}	F_{red}/F_{ox}
pure	777	37	124	3
K_1 (1:1)	780	3	38	12
K_1 (1:10)	780	26		
K_2 (1:1)	784	4	28	7
K_2 (1:10)	777	22		
(Frigaard et al., 1998) chlorosomes (1.2:10)	763			12
(Frigaard et al., 1997) chlorobiumquinone (1:10)	765			6.9

5 Discussion

5.1 Transient absorption spectra analysis

In transient absorption spectra there were observed a decrease of absorption of aggregated BChl *c* and Car and an increase of absorption of another components. The major features of the increasing part were: a broad peak at 960 nm; a broad peak at 850 nm; a peak at 820 nm; a peak at 700 nm; a peak at 560 nm; and a broad band starting at 550 nm and extending farther to blue.

By comparing the peak at 960 nm with the spectrum in fig. 27, we can ascribe it to increasing absorption of Car^+. The spectrum shown in fig. 27 belongs to spheroidene cation, whereas the carotenoid contained in chlorosome is chlorobactene, but both carotenoids have ten conjugated double bonds, ignoring the ring system, (see fig. 25), therefore we assume that their absorption spectra (and the absorption spectra of their cations) are similar.

The peaks at 850 nm and at 700 nm and the blue region band have strong resemblance to the chlorophyll a^+ spectrum (fig. 26). Therefore we have assigned these features to the increase of BChl c^+ absorption. Again, chlorophyll *a* and BChl *c* have similar structure, especially conjugated double bonds pattern (see fig. 1), implying similar absorption spectra.

Considering the fact that the peak at 820 nm was missing in the FCN sample spectrum and the role of $K_3[Fe(CN)_6]$ as an electron acceptor, this peak can be connected to semiquinone molecule, but because we do not have an absorption spectrum of semiquinone form of chlorobiumquinone we can not make this assignment.

The remaining positive peak at 560 nm can not be explained in these term, but considering its rather spiky shape, we think that it is some sort of artefact caused by spectra glueing.

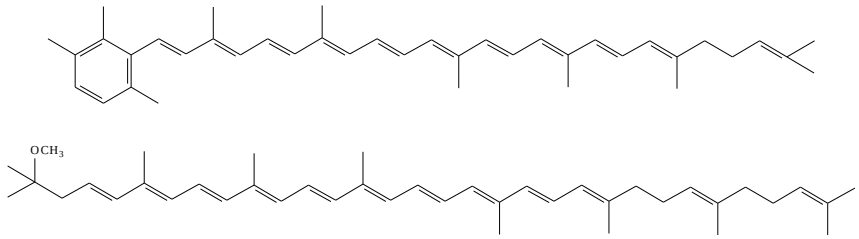

Figure 25: Chlorobactene structure (top) and spheroidene structure (bottom).

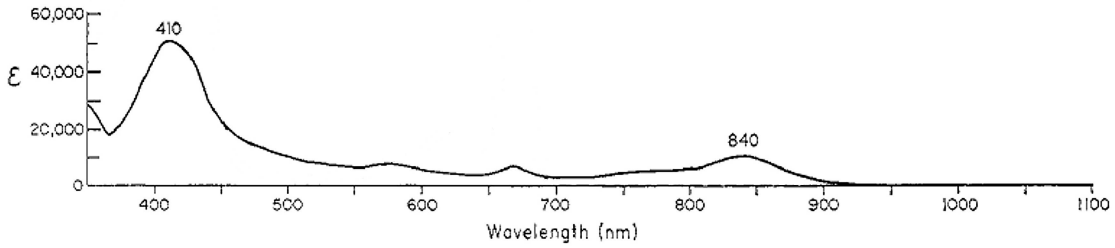

Figure 26: Chlorophyll a^+ spectrum, adapted from (Fuhrhop and Mauzerall, 1968)

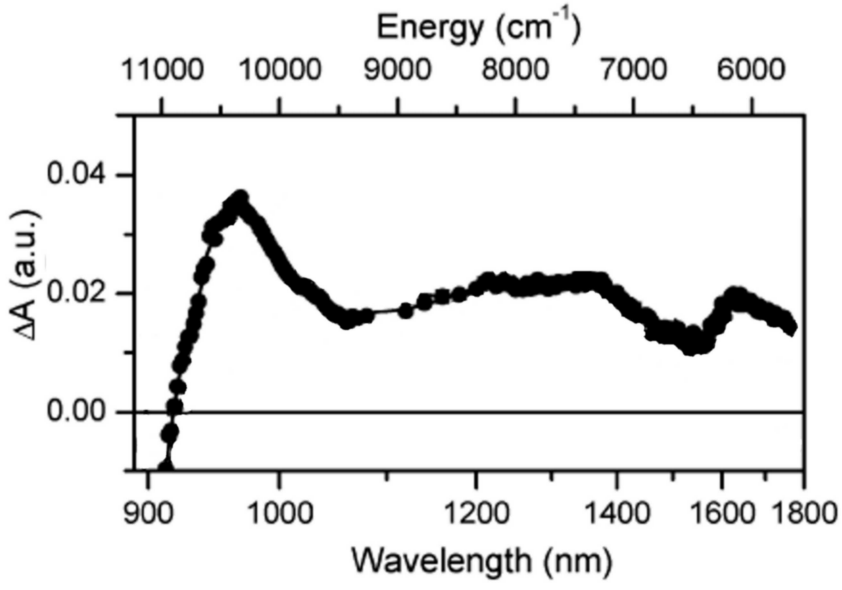

Figure 27: Car^+ spectrum, adapted from (Polívka et al., 2004)

5.2 Kinetics

As far as the kinetics parameters determination is concerned, we have focused mainly on the 750-900 nm region. The addition of $K_3[Fe(CN)_6]$ led to an increase of the transient absorption signal compared to aerobic conditions, whereas with addition of sodium dithionite the signal was negligible. For short actinic light exposures the signal to noise ratio was good enough to determine exponential component lifetime only for FCN samples, the values for normal samples were determined with a relatively large error, and values for Dit samples could not be determined at all. Moreover, as the detector sensitivity decreases in IR band, the errors increase for longer wavelengths. Longer actinic light exposures increased the amplitude of signal, but as the exponential component seems independent of the length of actinic light exposure, more precise values can be obtained only by averaging results from multiple experiments.

The acquired lifetimes of the exponential component of the linear-exponential model are summarized in table 4. It seems that addition of $K_3[Fe(CN)_6]$ shorten the lifetimes approx. to a half of the value obtained at aerobic conditions and that the lifetimes of dark relaxation are approx. 2-3 times longer than the lifetimes of actinic light response.

The reversibility of light induced changes is comparable for all samples within the experimental error. The exponential component is dominant for short actinic light exposure experiments. For longer actinic light exposures (~ 100 s) the reversibility is approx. 30 %.

The magnitude of signal in FCN samples is approx. 250 % and in Dit samples approx. 30 % of the signal in sample without additions.

Admittedly, these measurements are not precise enough to draw conclusions about actinic light response kinetics, and more measurements will be needed to do so, but none of the observations is in contradiction to our hypothesis.

Table 4: Lifetimes of exponential components of model. Values in italics are determined from only one measurement. Time in sample description indicate actinic light exposure length.

T_2 [s]

sample	750 nm	850 nm	967 nm
normal 7 s	0.78 ± 0.40	*3.53 ± 9.23*	*0.53 ± 0.84*
FCN 7 s	0.42 ± 0.11	0.41 ± 0.29	*0.36 ± 0.39*

T_5 [s]

sample	750 nm	850 nm	920 nm
normal 7 s	1.84 ± 0.91	*0.82 ± 0.66*	*0.60 ± 0.51*
FCN 7 s	1.17 ± 0.22	1.23 ± 0.58	*0.31 ± 0.26*

Table 5: Overall absorbance difference for dark part of experiment to overall absorbance difference for actinic light part of experiment ratio. Values in italics are determined from only one measurement. Time in sample description indicate actinic light exposure length.

$\Delta OD_{AC}/\Delta OD_{dark}$

sample	750 nm	850 nm	960 nm
normal 7 s	-0.42 ± 0.15	-0.58 ± 0.41	-0.82 ± 0.48
normal 80 s	*−0.33 ± 0.03*	*0.16 ± 0.18*	*−0.31 ± 0.26*
FCN 7 s	-0.56 ± 0.04	0.51 ± 0.20	
FCN 115 s	*−0.28 ± 0.02*	*−0.21 ± 0.02*	*−0.35 ± 0.51*
Dit 7 s	*−0.60 ± 0.53*	*−0.25 ± 0.59*	

Table 6: Comparison of additions effect on overall absorbance difference for actinic light part of the experiment. The values are related to normal 7 s (†) or normal 80 s (‡) ΔOD. Values in italics are determined from only one measurement. Time in sample description indicate actinic light exposure length.

$\Delta OD_{AC}/\Delta OD_{AC}^{normal}$

sample	750 nm	850 nm	960 nm
Dit7 s†	0.26 ± 0.23	1.2 ± 1.69	
FCN7 s†	1.58 ± 0.58	3.14 ± 1.71	*0.34 ± 0.23*
FCN115 s‡	2.66 ± 0.18	2.47 ± 0.49	*2.60 ± 0.57*

5.3 Role of quinones

The steady state absorption spectra (fig. 5) indicates that vitamins K_1 and K_2 promote forming of BChl *c* aggregates. It is even possible to form BChl *c*-vitamin K_1 (or K_2) aggregate without lipids. Moreover, the blue shift of the Q_y absorption maxima suggests that vitamins are incorporated into aggregates in close vicinity of BChl *c* and are able to modify the BChl *c*-BChl *c* interactions.

The fluorescence spectroscopy results (table 3) indicates that vitamins K_1 and K_2 are able to mediate an effective excitation energy quenching under aerobic conditions. These results are in accordance with published values (Frigaard et al., 1997), (Frigaard et al., 1998). Interestingly, the vitamins are able to achieve the same effect as, in the *Chlorobium tepidum* naturaly occuring, chlorobiumquinone, but are required in greater concentrations in order to do so. This may be caused by lack of 1' oxygen (see fig. 28), which has been suggested to have structural importance (Blankenship and Matsuura, 2003), possibly implying that vitamins are not in an optimal position in aggregates. Another possible explanation is that not all vitamins used for preparation are incorporated into aggregates.

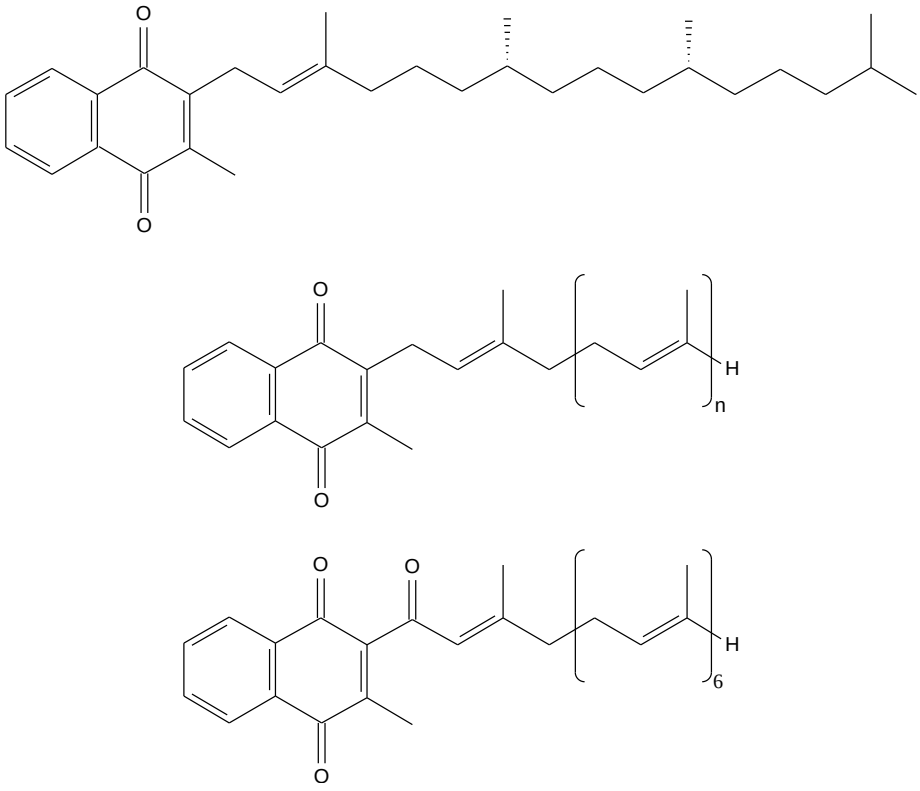

Figure 28: Vitamin K_1 structure (top), vitamin K_2 structure (middle; vitamin K_2 is in fact a mixture of molecules with n = 5, 6 or 9), and chlorobiumquinone structure (bottom).

6 Conclusion

Artificial aggregates of BChl *c* in aqueous environment can be formed using lipids and quinones not found in native chlorosome of green sulphur bacteria, namely lecithine and vitamins K_1 or K_2. The aggregates have similar spectral characteristics as chlorosomes. Incorporation of quinones into aggregate induct efficient excitation energy quenching at high redox potential as in chlorosomes.

Under aerobic conditions, photoinduced transient changes were observed in absorption spectra of chlorosomes. The changes corresponds to decrease of absorption of aggregated BChl *c* and Car and increase of absorption between 800–1000 nm. The data indicates that the signal with a maximum at ~ 850 nm is due to BChl *c* cation and the signal with a maximum at ~ 960 nm is due to chlorobactene cation. This attribution is supported by comparison with spectra of known cations of similar chlorophyll and carotenoid. Further, we observed that the signal is enhanced by addition of artificial electron acceptor ($K_3[Fe(CN)_6]$) and attenuated by addition of artificial electron donor (sodium dithionite), which also suggest that observed species are cations. The results indicate that photooxidation of BChl *c* leading to formation of BChl c^+ indeed occur in chlorosomes at aerobic conditions, in accordance with our working hypothesis. Part of the BChl c^+ may recombine by oxidation of Car leading to formation of Car^+.

References

Blankenship, R. E., Cheng, P., Causgrove, T. P., Brune, D. C., Wang, S. H.-H., Choh, J.-U., and Wang, J.: 1993, *Photochemistry Photobiology* **57(1)**, 103

Blankenship, R. E. and Matsuura, K.: 2003, in B. R. Green and W. W. Parson (eds.), *Light-Harvesting Antennas*, pp 195–217, Kluwer Academic Publishers, Dordrecht

Blankenship, R. E., Olson, J. M., and Miller, M.: 1995, in R. E. Blankenship, M. T. Madigan, and C. E. Bauer (eds.), *Anoxygenic photosynthetic bacteria*, pp 399–435, Kluwer Academic Publishers, Dordrecht

Frigaard, N.-U., Matsuura, K., Hirota, M., Miller, M., and Cox, R. P.: 1998, *Photosynthesis Research* **58**, 81

Frigaard, N.-U., Takaichi, S., Hirota, M., Shimada, K., and Matsuura, K.: 1997, *Archives of Microbiology* **167**, 343

Frigo, M. and Johnson, S. G.: 2005, *Proceedings of the IEEE* **93(2)**, 216, special issue on "Program Generation, Optimization, and Platform Adaptation"

Fuhrhop, J.-H. and Mauzerall, D.: 1968, *Journal of the American Chemical Society* **90**, 3875

Gerola, P. D. and Olson, J. M.: 1986, *Biochimica et Biophysica Acta* **848**, 69

Jones, E., Oliphant, T., Peterson, P., et al.: 2001, *SciPy: Open source scientific tools for Python*

Klinger, P., Arellano, J. B., Vacha, F., Hala, J., and Pšenčík, J.: 2004, *Photochemistry and Photobiology* **80**, 572

Polívka, T., Pullerits, T., Frank, H. A., Cogdell, R. J., and Sundstrom, V.: 2004, *Journal of Physical Chemistry B* **108(39)**, 15398

Pšenčík, J., Ikonen, T., Laurinmki, P., Merckel, M., Butcher, S., Serimaa, R. E., and Tuma, R.: 2004, *Biophysical Journal* **87**, 1165

Pšenčík, J., Ma, Y.-Z., Arellano, J. B., Hála, J., and Gillbro, T.: 2003, *Biophysical Journal* **84**, 1161

Valentin, M. D., Malorni, D., Maniero, A. L., Agostini, G., Giacometti, G., Vianelli, A., Vannini, C., Cattaneo, A. G., Brunel, L.-C., and Carbonera, D.: 2002, *Photosynthesis Research* **71**, 33

van Noort, P. I., Zhu, Y., LoBrutto, R., and Blankenship, R. E.: 1997, *Biophysical Journal* **72**, 316

Vassilieva, E. V., Antonkine, M. L., Zybailov, B. L., Yang, F., Jakobs, C. U., Golbeck, J. H., and Bryant, D. A.: 2001, *Biochemistry* **40**, 464

Wahlund, T. M., Woese, C. R., Castenholz, R. W., and Madigan, M. T.: 1991, *Archives of Microbiology* **156**, 81

A Tables

Table 7: Overall absorbance difference for actinic light part of experiment for individual samples (blue part of the spectrum). Time in sample description denotes actinic light exposure length. Each field contain parameter average, error and number of measurements considered during average computing.

$\Delta OD_{AC}[10^{-4}]$					
space	455 nm	505 nm	530 nm	672 nm	700 nm
FCN 115 s				-5.85 1.25 1	7.82 1.25 1
FCN 25 s				-2.23 1.24 1	0.71 0.8 2
FCN 7 s				-0.2 2.08 3	2.15 1.49 3
FCN 4 s					0.5 0.72 1
FCN 2 s				-0.83 1.05 1	1.82 1.56 1
normal 80 s	-25.93 0.8 4	-10.3 2.75 4	-1.1 0.64 1	-2.12 1.2 1	
normal 7 s				-2.64 1.01 9	-0.88 1.39 7
Dit 7 s	-0.96 1.11 1	6.86 3.45 1	-0.64 0.82 1		

Table 8: Overall absorbance difference for actinic light part of experiment for individual samples (red part of the spectrum). Time in sample description denotes actinic light exposure length. Each field contain parameter average, error and number of measurements considered during average computing.

$\Delta OD_{AC}[10^{-4}]$

space	750 nm	820 nm	850 nm	867 nm	920 nm	960 nm	967 nm
FCN 115 s	-92.22 5.3 2	7.52 0.76 2	11.53 0.71 4	8.42 0.78 2	8.62 1.29 1	14.89 1.25 1	
FCN 25 s	-38.93 2.66 2	1.51 1.54 2	5.07 1.14 2				
FCN 13 s						7.6 1.53 1	5.25 1.11 2
FCN 7 s	-23.13 6.4 5	-1.4 1.12 5	5.65 1.65 5		1.25 0.23 2	1.08 0.33 1	0.92 0.35 1
FCN 4 s	-17.44 1.16 2	-0.05 0.8 2	2.57 6.9 1				1.55 1.81 1
FCN 2 s	-9.99 9.97 4	1.32 1.05 1					
normal 195 s					2.61 0.82 6	4.46 0.43 3	4.55 0.43 3
normal 80 s	-34.73 1.18 2	7.1 0.84 2	4.67 0.88 2		3.62 0.87 4	5.72 1.15 1	5.05 1.33 1
normal 7 s	-14.66 3.48 38	2.57 2.84 23	1.8 0.83 27	-0.62 2.59 8	4.51 4.32 1	3.15 1.89 3	3.46 2.04 3
Dit 7 s	-3.77 3.21 8	0.89 2.86 3	2.16 2.85 5	-1.83 4.28 1			

Table 9: Overall absorbance difference for dark part of experiment for individual samples (red part of the spectrum). Time in sample description denotes actinic light exposure length. Each field contain parameter average, error and number of measurements considered during average computing.

$\Delta OD_{dark}[10^{-4}]$

space	750 nm	820 nm	850 nm	867 nm	920 nm	960 nm	967 nm
FCN 115 s	26.03 2.14 2		-2.58 2.29 2	-4.01 2.01 1	-3.6 2.59 1	-5.25 7.56 1	
FCN 25 s	17.22 2.17 2						
FCN 13 s							-3.37 1.41 2
FCN 7 s	13.66 2.85 4		-2.87 1.05 5		-5.21 0.91 2		-5.53 1.45 1
FCN 4 s	12.06 2.07 2						
FCN 2 s	9.11 7.33 4						
normal 195 s					-7.59 4.16 4	-9.11 11.67 1	
normal 80 s	11.6 1.0 2					-1.79 1.44 1	-2.77 1.74 1
normal 7 s	6.37 1.81 36				-1.71 3.4 1	-2.56 1.8 1	-2.56 1.8 1

Table 10: Amplitude of the exponential component of the model for actinic light part of experiment for individual samples (red part of the spectrum). Time in sample description denotes actinic light exposure length. Each field contain parameter average, error and number of measurements considered during average computing.

	A_2 $[10^{-4}]$						
sample	750 nm	820 nm	850 nm	867 nm	920 nm	960 nm	967 nm
FCN 115 s	18.39 2.03 2		-3.23 0.46 3	-2.65 0.94 2	-2.63 0.72 1		
FCN 25 s	13.62 1.77 2		-1.36 0.65 2				
FCN 13 s							-1.58 0.65 2
FCN 7 s	15.59 2.69 5		-3.29 0.77 4		-0.57 0.18 2	-0.44 0.25 1	-0.52 0.22 1
FCN 4 s	10.88 0.76 2		-1.98 3.01 1				
FCN 2 s	13.34 4.76 4						
normal 195 s					-0.63 0.08 4	-0.92 0.09 3	-0.85 0.09 3
normal 80 s	3.32 0.62 2		-4.38 0.56 2		-1.53 0.58 4	-2.77 0.72 1	-1.61 0.75 1
normal 7 s	8.48 2.12 37		-0.92 1.26 1		-3.29 1.9 1	-2.01 1.46 1	-2.01 1.46 1

Table 11: Amplitude of the exponential component of the model for dark part of experiment for individual samples (red part of the spectrum). Time in sample description denotes actinic light exposure length. Each field contain parameter average, error and number of measurements considered during average computing.

A_5 $[10^{-4}]$

sample	750 nm	820 nm	850 nm	867 nm	920 nm	960 nm	967 nm
FCN 115 s			4.81 2.95 2	5.83 14.38 1	3.75 1.74 1	7.74 5.12 1	
FCN 25 s	-9.49 1.5 2						
FCN 13 s							2.6 0.95 2
FCN 7 s	-10.81 4.3 4		2.74 1.48 5		0.38 0.22 2		
FCN 4 s	-8.27 1.24 2		6.05 5.77 1				
FCN 2 s	-8.83 0.89 4		1.91 1.57 4				
normal 195 s					0.62 0.52 4	0.89 1.49 1	
normal 80 s	-5.93 0.56 2					1.82 0.78 1	1.73 0.81 1
normal 7 s	-7.94 1.86 39		1.76 0.8 1		1.51 0.81 1	1.77 0.83 1	1.77 0.83 1

Table 12: Lifetime of the exponential component of the model for actinic light part of experiment for individual samples (red part of the spectrum). Time in sample description denotes actinic light exposure length. Each field contain parameter average, error and number of measurements considered during average computing.

	T_2 [s]						
sample	750 nm	820 nm	850 nm	867 nm	920 nm	960 nm	967 nm
FCN 115 s	3.96 0.34 2		4.07 1.78 3	2.19 1.49 2	5.94 3.76 1		
FCN 25 s	0.32 0.03 2		2.01 2.37 1				
FCN 13 s							0.64 0.73 2
FCN 7 s	0.42 0.11 5		0.41 0.29 4				0.36 0.39 1
FCN 4 s	0.23 0.03 2		0.75 1.56 1				
FCN 2 s	0.54 0.22 4						
normal 195 s					6.09 4.12 4	8.64 4.24 3	6.52 4.46 3
normal 80 s	0.09 0.07 1		5.7 1.8 2		3.15 3.35 1	1.82 1.87 1	4.17 5.17 1
normal 7 s	0.78 0.4 37		3.53 9.23 1		1.11 1.34 1	0.53 0.84 1	0.53 0.84 1

Table 13: Lifetime of the exponential component of the model for dark part of experiment for individual samples (red part of the spectrum). Time in sample description denotes actinic light exposure length. Each field contain parameter average, error and number of measurements considered during average computing.

	T_5 [s]						
sample	750 nm	820 nm	850 nm	867 nm	920 nm	960 nm	967 nm
FCN 115 s			7.66 6.59 2	26.8 64.91 1	5.72 6.34 1	16.59 14.77 1	
FCN 25 s	1.44 0.65 2						
FCN 13 s							1.93 1.11 2
FCN 7 s	1.17 0.22 4		1.23 0.58 4		0.31 0.26 2		
FCN 4 s	1.46 0.32 2		2.92 2.97 1				
FCN 2 s	1.47 0.27 4		1.72 2.1 4				
normal 195 s					19.5 16.27 4	28.96 42.1 1	50.0 137.6 1
normal 80 s	8.21 2.46 2					7.25 6.63 1	12.04 12.13 1
normal 7 s	1.84 0.91 37		0.82 0.66 1		0.6 0.51 1	0.51 0.35 1	0.51 0.35 1

Table 14: Overall absorbance difference for dark part of experiment to overall absorbance difference for actinic light part of experiment ratio for individual samples (blue part of the spectrum). Time in sample description denotes actinic light exposure length. Each field contain parameter average, error and number of measurements considered during average computing.

$\Delta OD_{dark}/\Delta OD_{AC}$

sample	455 nm	505 nm	530 nm	672 nm	700 nm
FCN 115 s					-0.11 0.18 1
FCN 25 s					1.67 3.85 2
FCN 7 s				0.35 0.96 1	-0.7 0.93 3
FCN 4 s					-1.93 3.51 1
normal 80 s	0.18 0.04 4	0.85 0.51 4	6.67 4.12 1	-1.42 1.0 1	
normal 7 s				-0.68 0.58 7	-0.45 0.68 1
Dit 7 s	2.4 3.09 1	0.11 0.22 1	-1.43 2.3 1		

Table 15: Overall absorbance difference for dark part of experiment to overall absorbance difference for actinic light part of experiment ratio for individual samples (red part of the spectrum). Time in sample description denotes actinic light exposure length. Each field contain parameter average, error and number of measurements considered during average computing.

$\Delta OD_{dark}/\Delta OD_{AC}$

	750 nm	820 nm	850 nm	867 nm	920 nm	960 nm	967 nm
FCN 115 s	-0.28 0.02 2	0.18 0.2 1	-0.21 0.2 2	-0.5 0.26 1	-0.42 0.31 1	-0.35 0.51 1	
FCN 25 s	-0.44 0.06 2						
FCN 13 s						-0.34 1.01 1	-0.65 0.32 2
FCN 7 s	-0.56 0.04 4	0.8 1.03 3	-0.51 0.2 5		-4.17 1.05 2		-5.99 2.78 1
FCN 4 s	-0.69 0.13 2						
FCN 2 s	-0.91 1.19 4	-2.1 1.94 1					
normal 195 s					-1.7 0.76 6	-1.06 1.21 3	-0.33 0.38 1
normal 80 s	-0.33 0.03 2	-0.29 0.27 2	0.16 0.18 2			-0.31 0.26 1	-0.55 0.37 1
normal 7 s	-0.42 0.15 36	-1.02 1.95 14	-0.58 0.41 20	-0.85 1.32 8	-0.38 0.84 1	-0.82 0.48 2	-0.68 1.1 2
Dit 7 s	-0.6 0.53 1	-0.4 0.94 1	-0.25 0.59 1				

Table 16: Overall absorbance difference for dark part of experiment to overall absorbance difference for actinic light part of experiment ratio interpolated for 60 actinic light exposure for individual samples (red part of the spectrum). Time in sample description denotes actinic light exposure length. Each field contain parameter average, error and number of measurements considered during average computing.

$\Delta OD^{60\,s}_{dark}/\Delta OD^{60\,s}_{AC}$

sample	750 nm	820 nm	850 nm	867 nm	920 nm	960 nm	967 nm
FCN 115 s	-0.4 0.02 2		-0.39 0.26 2	-0.68 0.37 1	-0.61 0.42 1		
FCN 25 s	-0.41 0.08 2						
FCN 13 s							-0.18 0.14 2
FCN 7 s	-0.17 0.04 4		-0.12 0.1 4		-2.29 0.56 2		-4.28 2.14 1
FCN 4 s	-0.15 0.07 2						
FCN 2 s	0.13 0.3 1						
normal 195 s					-4.45 3.59 1	-3.85 4.76 1	
normal 80 s	-0.3 0.03 2					-0.46 0.25 1	-0.6 0.37 1
normal 7 s	-0.11 0.12 34					-0.09 0.1 1	-0.09 0.1 1